Spatial and temporal variations of tap water ^{17}O-excess in China

Chao Tian[a], Lixin Wang[a, *], Fuqiang Tian[b], Sihan Zhao[b] and Wenzhe Jiao[a]

[a] Department of Earth Sciences, Indiana University-Purdue University Indianapolis (IUPUI), IN 46202, USA

[b] Department of Hydraulic Engineering, State Key Laboratory of Hydroscience and Engineering, Tsinghua University, Beijing 100084, P. R. China

* Corresponding author contact information: Lixin Wang, Department of Earth Sciences, Indiana University-Purdue University Indianapolis, Indianapolis, IN, 46202, USA. Tel.: 317-274-7764. Fax: 317-274-7966

E-mail address: tianchao9996@163.com (C. Tian), lxwang@iupui.edu (L. Wang), tianfq@tsinghua.edu.cn (F. Tian), zhaosihan10@163.com (S. Zhao), wenzjiao@iu.edu (W. Jiao)

This is the author's manuscript of the article published in final edited form as:

Tian, C., Wang, L., Tian, F., Zhao, S., & Jiao, W. (2019). Spatial and temporal variations of tap water 17O-excess in China. Geochimica et Cosmochimica Acta. https://doi.org/10.1016/j.gca.2019.06.015

Compared to tap water δ^2H and $\delta^{18}O$, tap water ^{17}O-excess preserves additional information about source water dynamics. In this study, we provide the first report of ^{17}O-excess variations of tap water across China (652 samples). Annual ^{17}O-excess of tap waters at the national scale did not show obvious spatial pattern, and was almost unaffected by local environmental factors except in the Qinghai-Tibet Plateau region with a strong latitudinal trend. The mean ^{17}O-excess values in different seasons were not significantly different. The isotopic compositions of most of the tap waters at the annual and seasonal scale were likely influenced by the equilibrium fractionation effect ($\delta'^{18}O$-$\delta'^{17}O$ slope ranged from 0.5277 to 0.5301), except for the northwest region in the summer (slope = 0.5264) influenced by kinetic fractionation associated with re-evaporation effect. Based on the information of tap water source distribution, site aridity index and the known precipitation $\delta^{18}O$ values, a subset of the tap water can be considered as precipitation proxy. Different from the obvious spatial characteristics of precipitation $\delta^{18}O$, precipitation ^{17}O-excess did not show a clear spatial pattern. But it revealed much detailed precipitation formation mechanisms related to different climate regions and geographical conditions. The lower ^{17}O-excess values of the precipitation-sourced tap waters were caused by kinetic fractionation associated with supersaturation process in snow or glacier formation and re-evaporation effect in some arid regions. The higher ^{17}O-excess values of the precipitation-sourced tap waters in the inland were caused by continental moisture recycling, while likely caused by multiple factors in the southeast coastal region including short transport from ocean source and the humid local environment. Overall, this study provides a unique tap water ^{17}O-excess dataset across China, and probes the precipitation formation mechanisms using tap waters.

Key words: ^{17}O-excess; precipitation; tap water; stable isotopes

1. INTRODUCTION

Stable isotopes of hydrogen and oxygen (δ^2H, $\delta^{18}O$, and $\delta^{17}O$) are powerful tracers to probe ecohydrological and hydroclimatic processes experiencing equilibrium and kinetic fractionation during phase change (e.g., evaporation, condensation, and sublimation) (Angert et al., 2004; Jameel et al., 2016; Tian et al., 2016; Wang et al., 2010; Zhao et al., 2012). A new isotope tracer ^{17}O-excess ($^{17}O\text{-excess} = \ln(\delta^{17}O + 1) - 0.528 \times \ln(\delta^{18}O + 1)$) becomes available in recent years providing opportunities for a better understanding of the mechanisms of multiple hydrological and meteorological processes (Barkan and Luz, 2007; Berman et al., 2013; Steig et al., 2014). The d-excess (d-excess = $\delta^2H - 8 \times \delta^{18}O$) and ^{17}O-excess are both sensitive to the kinetic fractionation (e.g., evaporation and condensation in supersaturation condition) (Landais et al., 2012a; Li et al., 2015; Li et al., 2017). The d-excess is sensitive to both temperature and relative humidity (hereafter RH), while ^{17}O-excess is theoretically mainly affected by RH because the effects of temperature on $\delta^{18}O$ and $\delta^{17}O$ partially cancel each other out during 10°C to 45°C (Barkan and Luz, 2005, 2007; Jacob and Sonntag, 1991). For example, ^{17}O-excess of monsoon precipitation and leaf water in Africa are both only sensitive to the RH at the precipitation site (Landais et al., 2010; Li et al., 2017). ^{17}O-excess in subtropical island precipitation and coastal East Antarctica ice cores are both affected by RH at the oceanic source region (Uechi and Uemura, 2019; Winkler et al., 2012). On the other hand, ^{17}O-excess of snow in Antarctica is affected by atmospheric temperature through kinetic fractionation associated with supersaturation conditions under extremely cold condition (Landais et al., 2012a; Pang et al., 2015; Schoenemann et al., 2014). Moreover, the latitudinal variation of ^{17}O-excess among tap waters reflects the different controls on precipitation ^{17}O-excess in different regions across the continental United States (U.S.) (Li et al., 2015). Overall, the studies of ^{17}O-excess variations at large spatiotemporal scales have mainly focused on high-latitude

regions including research on seasonal variation of snow (Landais et al., 2012a; Landais et al., 2012b), spatial distribution of snow (Pang et al., 2015), and paleoclimate reconstruction on ice cores (Schoenemann et al., 2014; Winkler et al., 2012). Until now, water ^{17}O-excess in the mid-latitude regions have been observed only in temporal variations of precipitation in the central U.S. (Tian and Wang, 2019; Tian et al., 2018) and Switzerland (Affolter et al., 2015), and spatial variations of tap water in the U.S. (Li et al., 2015).

Tap water is an important part of the domestic water use, directly linking anthropogenic and hydrological systems. Previous studies showed that the tap water with similar isotope variations to the precipitation can be used as a proxy to study the local precipitation (Bowen et al., 2007, West et al., 2014). Therefore, the proxy method provides a window to study precipitation isotopic variations using tap water when precipitation samples are not available. The distribution of water sources in China is uneven, abundant water is concentrated in the south while it is drier in the north with extensive water-intensive economic activities (e.g., coal mining and wheat cultivation) (Nickum, 1998; Piao et al., 2010). Moreover, precipitation patterns could be affected by climate change, which will make the uneven distribution of water resources even worse (McDonald et al., 2011). As such, water scarcity caused by economic development, population growth and climate change is regarded as one of the most important threats for sustainable development of human societies (Gohari et al., 2013; Pekel et al., 2016). Therefore, it is useful to understand the spatial and temporal variations of tap water isotopic compositions to inform water-resource management strategies (Jameel et al., 2016; West et al., 2014).

Here, we investigated tap water ^{17}O-excess variations from 92 cities across China, analyzed the spatial and seasonal variations, and examined the effects of geographical (e.g., longitude, latitude, and altitude) and meteorological factors (e.g., precipitation amount, temperature, and RH)

on ^{17}O-excess variations. In addition, we investigated whether the tap water could be served as a proxy for the precipitation by combining information of tap water source distribution, site aridity index and the known precipitation $\delta^{18}O$ values. The precipitation ^{17}O-excess variations and the relationships with environmental factors were also studied to better reveal the precipitation formation mechanisms.

2. MATERIALS AND METHODS

2.1. Tap water sample collections

The tap water samples were collected every month in 2015 (from December 2014 to November 2015) across 31 provinces (95 sites) almost covering all the 34 provinces in China (780 samples). The details of the collecting process have been reported by Zhao et al. (2017). The samples were delivered to the IUPUI (Indiana University-Purdue University Indianapolis) Ecohydrology Lab to measure $\delta^{18}O$ and $\delta^{17}O$ for ^{17}O-excess quantification after the conventional isotope ($\delta^{2}H$ and $\delta^{18}O$) measurements in Hydrology Laboratory of Tsinghua University. These samples were stored in a refrigerator at 4^{o}C until isotope analysis. 652 samples from 92 locations in 30 provinces (except Beijing, Zunyi, and Qinzhou) were analyzed for ^{17}O-excess and triple isotope compositions ($\delta^{2}H$, $\delta^{18}O$, and $\delta^{17}O$) at IUPUI due to some sample loss in transportation, which means some cities had only sporadic samples in fewer months (Figs. 1-2).

2.2. Isotope analysis and ^{17}O-excess data processing

The isotopic ratios ($\delta^{2}H$, $\delta^{18}O$, and $\delta^{17}O$) of all the tap water samples were concurrently determined at IUPUI Ecohydrology Lab using the methods of Tian et al. (2016) and Wang et al. (2009). In brief, the samples were measured at 1 Hz using a Triple Water Vapor Isotope Analyzer (T-WVIA-45-EP; Los Gatos Research Inc. (LGR), Mountain View, CA, USA) coupled to a Water Vapor Isotope Standard Source (WVISS, LGR, Mountain View, CA, USA). T-WVIA and WVISS

was preheated to 50°C and 80°C, respectively, to obtain higher accuracy and precision, and pipe-heating cable was used to heat the Teflon tubing connecting the two instruments to avoid condensation of water vapor. All the samples were measured under 13000 ppm under which higher performance was observed (Tian et al., 2016) and run for about 2 min, so 120 data points were attained for each sample.

To ensure the accuracy of measurement, five working standards from LGR with known isotopic composition (with a range of -154.0‰ to -9.2‰, -19.49‰ to -2.69‰, and -10.30‰ to -1.39‰ for δ^2H, $\delta^{18}O$, and $\delta^{17}O$, respectively) were analyzed routinely after every five samples. Moreover, two international water standards Vienna Standard Mean Ocean Water (V-SMOW) and Standard Light Antarctic Precipitation (SLAP) were used to normalize all of the isotope ratios following the procedure described by Steig et al. (2014) and Schoenemann et al. (2013), where $\delta^2H_{SLAP/VSMOW}$ = -427.50‰, $\delta^{18}O_{SLAP/VSMOW}$ = -55.50‰, $\delta^{17}O_{SLAP/VSMOW}$ = -29.6986‰. They were measured once during each day of the measurements.

To attain accurate ^{17}O-excess measurements, for each sample (about 120 data points), one λ value ($\lambda = \ln(\delta^{17}O + 1) / \ln(\delta^{18}O + 1)$) and one ^{17}O-excess value were calculated for each individual data point as a quality control filter (Barkan and Luz, 2005; Meijer and Li, 1998). The λ value is the same as mass-dependent fractionation coefficient (θ) during liquid-vapor equilibrium and water vapor diffusion in air (Angert et al., 2004; Meijer and Li, 1998). Any measurements outside the theoretical kinetic and equilibrium fractionation coefficient (θ) range (i.e., $\lambda = \theta$ when θ is between 0.506 and 0.530) or outside the observed ^{17}O-excess range in global precipitation (-100 to +100 per meg) (1 per meg = 0.001‰) were treated as outliers (Angert et al., 2004; Barkan and Luz, 2005; Landais et al., 2010; Li et al., 2015; Luz and Barkan, 2010). The ^{17}O-excess final value was the mean value of quality-controlled data. The precision (i.e., standard deviation of three

measurements for the same sample) of our OA-ICOS technique was <0.80‰, <0.06‰, <0.03‰, and <12 per meg for δ^2H, $\delta^{18}O$, $\delta^{17}O$, and ^{17}O-excess, respectively (Table A1). Out of seven standards used, six showed ^{17}O-excess precisions were better than 8 per meg (Table A1). The precision range (2 to 12 per meg) in our study is comparable with IRMS technique (4 to 13 per meg) (Berman et al., 2013; Li et al., 2015; Luz and Barkan, 2010; Pang et al., 2015; Schoenemann et al., 2013) and CRDS method (<10 per meg) (Affolter et al., 2015; Steig et al., 2014).

2.3. Tap water suitable as precipitation proxy

To estimate the spatial variations of precipitation ^{17}O-excess in China, tap water samples were filtered to select the ones that could be used as precipitation proxy based on the tap water source together with site aridity and the $\delta^{18}O$ value comparison between precipitation and tap water. Surface water is one of the most important water resources for tap water, which is constantly and directly replenished by precipitation. Previous studies demonstrated that surface waters (e.g., river water in northern Central America and stream water in Japan), to some extent, are good proxies of precipitation (Katsuyama et al., 2015; Lachniet and Patterson, 2009). In this study, 23 surface water-dominated sites were first selected from 92 tap water sites based on the national water supply census data in 2011. To evaluate the degree of dryness in a site, aridity index values were extracted from the Global Aridity Index dataset (https://cgiarcsi.community/data/global-aridity-and-pet-database/). Aridity index of the 23 surface water-dominated sites ranged from 0.12 to 1.29 (Table A2). Four sites with aridity index less than 0.5 (Longnan, Pingliang, Delingha, and Baotou) were removed to avoid the effects of strong evaporation on isotopic compositions. Consequently, tap waters from 19 surface water-dominated sites were used as proxies for precipitation in our study.

To increase the number of samples that could be potentially used as precipitation and increase spatial coverage, the mean annual $\delta^{18}O$ values of the observed tap water were compared

with the mean annual precipitation $\delta^{18}O$ from the Global Network of Isotopes in Precipitation (GNIP) and Chinese Network of Isotopes in Precipitation (CHNIP) stations (Araguás-Araguás et al., 1998; Johnson and Ingram, 2004; Liu et al., 2014; Zhao et al., 2012). Twenty-four GNIP/CHNIP stations (22 stations from GNIP and 2 stations from CHNIP (Shijiazhuang and Shenyang)) were overlapped with our tap water sampling sites. Out of the 24 overlapping sites, eight sites (including Fuzhou which was already considered as precipitation based on the surface waters-dominated scenario) were considered as precipitation proxy because the $\delta^{18}O$ difference between the tap water and precipitation was less than ±0.5‰ (Table 1). Overall, tap waters from 26 sites, including 19 sites based on surface water domination and 8 sites based on small $\delta^{18}O$ differences (<0.5‰) (Fuzhou was chosen based on both scenarios), were considered as precipitation proxy and used to examine precipitation $\delta^{17}O$ characteristics (Fig. 1).

2.4. Geographical and meteorological variables

To interpret the ^{17}O-excess variations of tap water and examine precipitation formation mechanisms using isotopes, geographical and local meteorological data (http://data.cma.cn/) were obtained from Zhao et al. (2017), including the longitude, latitude, and altitude as well as mean annual precipitation amount, mean annual temperature, and mean annual relative humidity (hereafter MAP, MAT, and MARH from December 2014 to November 2015). The relationships between isotopic variations and environmental factors were used to evaluate whether single or combined local environmental factors affect the ^{17}O-excess variations using simple linear regression analysis and stepwise regression analysis in our study.

3. RESULTS

3.1. ^{17}O-excess variations of tap water

The monthly tap water ^{17}O-excess varied significantly between 19 and 66 per meg across China (652 samples), with a mean value of 39±8 per meg. It had the lowest value in May in Dalian and the highest value in May in Kaifeng (Fig. A1). Not every month was sampled for all the sites. Therefore, when examining the spatial differences, we focused on the annual scale to minimize the influences of seasonal difference among different regions. The ^{17}O-excess spatial variations of the annual tap water (92 sites) varied between 26 and 55 per meg, with the same mean value (39±5 per meg) as the monthly one (Table 2 and Fig. 1). The relatively low annual ^{17}O-excess values were obtained from Heihe and Harbin (26 and 28 per meg), as well as from the Qinghai-Tibet Plateau (hereafter QP) region (Lhasa and Nyingchi; 31 and 33 per meg, respectively) (Fig. 1 and A1). The relatively high annual ^{17}O-excess values (46 to 55 per meg) were mainly obtained from the southeast coastal area including Hangzhou, Hefei, Guangzhou, Zhanjiang, Yueyang, and Enshi (Fig. 1 and A1). The high ^{17}O-excess values were also observed in some inland cities (e.g., Shijiazhuang, Changchun, Baotou, and Dongying; 46 to 48 per meg) (Fig. 1 and A1). Note that the ^{17}O-excess values of Harbin (28 per meg) and Changchun (48 per meg), two nearby cities, were quite different (Fig. 1 and A1). To evaluate the ^{17}O-excess variation at the regional scale, the data were divided into six geographical regions (i.e., northern, northeastern, northwestern, QP, southeastern, and southwestern region, hereafter N, NE, NW, QP, SE, and SW) based on climate, following Zhao et al. (2017) (Table 2). ^{17}O-excess variations ranged from 35±7 to 42±5 per meg across the six regions (Table 2).

Tap water samples from each site were divided into four seasons to investigate the seasonal difference of ^{17}O-excess for both the national level and in six different regions (Table 3 and Fig.

2). ^{17}O-excess values of tap water at the national level in different seasons was between 38±6 and 40±8 per meg. For the six different regions, there was no obvious ^{17}O-excess difference between seasons with differences ranging from 2 per meg (from 38±5 to 40±8 per meg in N region) to 7 per meg (from 35±7 to 42±6 per meg in NW region).

The $\delta'^{18}O$-$\delta'^{17}O$ slopes (i.e., the slopes of 1000 x ln ($\delta^{18}O$ +1) and 1000 x ln ($\delta^{17}O$ + 1)) for annual tap waters at the national scale and in the six regions were between 0.5281 and 0.5293 (Fig. 3). The $\delta'^{18}O$-$\delta'^{17}O$ slopes of tap waters at the national scale were similar among different seasons (0.5288 to 0.5294) (Table 3 and Fig. 4). For the six different regions, almost all of the slopes were between 0.5277 to 0.5301 in different seasons except the one in the summer from the NW region with the lowest slope of 0.5264 (Table 3).

There were weak correlations between tap water ^{17}O-excess and latitude, MAT, MAP, and MARH at the national scale ($R^2 < 0.10$, $p < 0.05$ for all cases) (Fig. 5), similar to d-excess (Table A3). $\delta^{18}O$ exhibited much stronger correlations with the above factors ($R^2 = 0.16$-0.32, $p < 0.001$ for all cases) (Table A3). The linear stepwise regression model exhibited weak correlation between ^{17}O-excess and MAP ($R^2 = 0.08$, $p = 0.006$), while d-excess and $\delta^{18}O$ were both affected by multiple factors with stronger correlations ($R^2 = 0.39/0.46$, $p < 0.001$) (Table A4). There was no relationship between ^{17}O-excess and environmental factors in five regions except QP region. The ^{17}O-excess in the QP region was positively correlated with latitude ($R^2 = 0.89$, $p = 0.005$, n = 6) based on either simple linear regression model or stepwise regression model (Fig. 6A and Table A4). The $\delta^{18}O$ variations in the QP region were correlated with both latitude and altitude ($R^2 = 0.84$, $p < 0.05$ for both cases) and d-excess variation was correlated with altitude through the stepwise regression analysis ($R^2 = 0.82$, $p = 0.013$) (Fig. 6B-C and Table A4). The simple linear regression analysis and stepwise regression analysis both demonstrated that the ^{17}O-excess

variation in the summer from the NW region was negatively correlated with the summer temperature (R^2 = 0.79, p = 0.043), and $\delta^{18}O$ variation was negatively correlated with summer precipitation (R^2 = 0.79, p = 0.042) (Table A4).

3.2. Tap water as precipitation proxy

Twenty-six tap water samples were considered as precipitation proxy (hereafter precipitation) based on the criteria listed in the Methods. ^{17}O-excess variations of the 26 precipitation samples ranged from 26 to 48 per meg, with the mean value of 40±5 per meg (Fig. 1 and Table 4). The precipitation of the 26 sites covered all six regions. The ^{17}O-excess variations in the NE region ranged from 26 to 48 per meg with an average of 37±16 per meg, similar to the mean values in QP and SW regions (34 to 38 per meg). The mean values were 43, 42±4, and 42 per meg in the NW, SE, and N regions, respectively (Table 4).

The slope of $\delta'^{18}O$-$\delta'^{17}O$ in precipitation at the national scale was 0.5292±0.0003 (Fig. 7). The relationships between the precipitation isotopic variations and the local environmental factors were analyzed to examine the key drivers of the precipitation ^{17}O-excess variations and precipitation formation mechanisms. The results showed that the precipitation ^{17}O-excess at the national scale was weakly and negatively correlated with altitude (R^2 = 0.21, p = 0.02) based on either simple linear regression analysis or stepwise regression analysis, while d-excess had no correlation with local environmental factors (Table A4 and A5). $\delta^{18}O$ values were correlated to all six environmental factors (R^2 = 0.17-0.69, $p < 0.05$ for all cases) (Table A5), and stepwise regression model showed the importance of MAP and MARH on $\delta^{18}O$ (R^2 = 0.77, $p < 0.001$) (Table A4). To examine if the weak correlation between ^{17}O-excess and altitude was caused by the high altitude in the QP region, three sites from the QP region (Lhasa, Nyingchi, and Gannan) were excluded to re-examine the relationships between local environmental factors and

256 precipitation isotope variations. The results showed that ^{17}O-excess had no correlation with the six
257 environmental factors tested. The d-excess was still correlated with MAP ($R^2 = 0.17$, $p < 0.05$)
258 (Table A4 and A5). The $\delta^{18}O$ values were still correlated to four environmental factors (latitude,
259 MAT, MAP, and MARH) ($R^2 = 0.41$-0.61, $p < 0.05$ for all cases) (Table A5), and stepwise
260 regression model showed the importance of MAT and MAP on $\delta^{18}O$ ($R^2 = 0.70$, $p < 0.001$) (Table
261 A4).

262 To determine the specific influencing factors in six different regions, correlations between
263 annual ^{17}O-excess ($\delta^{18}O$) and local environmental factors were analyzed in the SE and SW regions,
264 while the other four regions were not analyzed due to low precipitation sample numbers ($n < 4$).
265 No correlations between ^{17}O-excess ($\delta^{18}O$) and the environmental factors were observed in the SE
266 and SW regions. However, d-excess in the SE region had negative correlation with MARH ($R^2 =$
267 0.34, $p = 0.035$, $n = 13$) (Table A4 and A5). The d-excess in the SW region had positive correlation
268 with latitude ($R^2 = 0.77$, $p = 0.021$, $n = 6$) (Table A5), and the stepwise regression analysis
269 exhibited the importance of latitude and altitude on d-excess ($R^2 = 0.995$, $p < 0.001$) (Table A4).
270

271 **4. DISCUSSION**

272 **4.1. Tap water ^{17}O-excess variations**

273 *4.1.1. Spatial characteristics*

274 The low ^{17}O-excess values of annual tap water were observed in some high latitude (Heihe
275 and Harbin) and high altitude (QP region; Lhasa and Nyingchi) regions. As previously reported,
276 extremely low $\delta^{18}O$ values of annual tap water from these sites are explained to some extent by
277 the low temperature due to the high latitude and high altitude (Zhao et al., 2017). However,
278 generally, ^{17}O-excess variation should not be temperature-dependent, except when extreme low

279 temperature condensation occurs leading to the low ^{17}O-excess values under supersaturation
280 conditions (e.g., in Antarctica) (Barkan and Luz, 2005; Schoenemann et al., 2014; Uemura et al.,
281 2010). Additionally, even ^{17}O-excess variation in the middle latitude has a correlation with
282 temperature, it is found to be negatively correlated with temperature (e.g., in Switzerland) (Affolter
283 et al., 2015). Similarly, it is observed that snow and cold-season rainfall lead to high ^{17}O-excess in
284 the northern U.S. (Li et al., 2015). In our study, the low ^{17}O-excess values (26 to 33 per meg) and
285 high ^{17}O-excess values (e.g., Urumqi and Changchun; 43 and 48 per meg) all corresponded to
286 relatively low temperature (2.0°C to 9.5°C vs 3.5°C to 6.9°C). Therefore, the low ^{17}O-excess values
287 of annual tap water from high latitude (Heihe and Harbin) and high altitude (Lhasa and Nyingchi)
288 regions in China is not likely caused by local temperature but by different control factors (e.g.,
289 different water sources). The relatively high ^{17}O-excess values of annual tap waters at the coastal
290 regions relative to the continental regions reflect a certain degree of the "continental effect",
291 similar to that the conventional isotopic compositions ($\delta^{18}O$ and $\delta^{2}H$) in precipitation decrease
292 with the increasing distance from the coast to the inland (Dansgaard, 1964; Rozanski et al., 1993).
293 Therefore, the high ^{17}O-excess values at the coastal regions might be caused by being adjacent to
294 the oceanic moisture and experiencing relatively short moisture trajectories (Liu et al., 2014). On
295 the other hand, there were high ^{17}O-excess values in some inland cities, which are likely influenced
296 by low RH of the ocean moisture sources, or by greater amounts of continental moisture recycling
297 in the relatively arid regions (e.g., northwest region), or by low temperature in the relatively cold
298 regions (e.g., northeast region) as mentioned in the U.S. (Li et al., 2015). Additionally, ^{17}O-excess
299 values showed considerable difference even in the nearby cities (e.g., Harbin and Changchun),
300 indicating different water source mixing. Therefore, ^{17}O-excess values of tap waters in China did
301 not show obvious spatial pattern, similar to d-excess while different from the $\delta^{18}O$ trend

(continental effect) (Zhao et al., 2017). Meanwhile, the $\delta'^{18}O$-$\delta'^{17}O$ slope for annual tap waters at the national scale (0.5290±0.0002) (Fig. 3) is close to that of Global Meteoric Water Line (GMWL) (0.528) (Luz and Barkan, 2010) and equilibrium fractionation coefficient of the vapor-liquid equilibrium (0.529±0.001) (Barkan and Luz, 2005). Moreover, different from $\delta^{18}O$, the ^{17}O-excess of the tap waters at the national scale were almost unaffected by local environmental factors.

^{17}O-excess values at the regional scale had no obvious differences between regions (35±7 to 42±5 per meg) (Table 2), showing different trend with the U.S. tap water (Li et al., 2015). There are relatively low ^{17}O-excess values in the Gulf states (the most southerly U.S.) and higher in the north of the U.S. This might be because 70% of the tap waters are sourced from precipitation in the U.S., where ^{17}O-excess has relationship with latitude (Li et al., 2015), while only about 28% of the tap waters were sourced from precipitation in our study. Additionally, there are different precipitation mechanisms due to the differences in environmental factors between the two countries. The $\delta'^{18}O$-$\delta'^{17}O$ slopes for annual tap waters in the six regions (0.5281 to 0.5293) are all similar to the equilibrium fractionation coefficient of the vapor-liquid transition (0.529±0.001) (Barkan and Luz, 2005) and the vapor-solid equilibrium (0.5285~0.5290) (Van Hook, 1968) (Fig. 3). It was interesting that only tap water ^{17}O-excess in the QP region (31 to 43 per meg) had significant positive correlation with latitude (Fig. 6A). Moreover, the altitude effect of $\delta^{18}O$ variations in the QP region (-0.7‰/100 m for altitude) (Fig. 6C) is similar to that of the precipitation (-0.30‰/100 m) (Liu et al., 2014).

4.1.2. Seasonal characteristics

There was no obvious ^{17}O-excess seasonal trend at the national level (38±6 to 40±8 per meg) (Table 3), similar to the $\delta^{18}O$ trend (Zhao et al., 2017). Moreover, the ^{17}O-excess of tap waters at the national scale were all affected by equilibrium effect at different seasons because of the similar

$\delta'^{18}O$-$\delta'^{17}O$ slopes of tap waters (0.5288 to 0.5294) (Fig. 4) (Barkan and Luz, 2005; Van Hook, 1968). Tap water ^{17}O-excess seasonal trends was negligible in all the six regions with small seasonal difference (2 to 7 per meg) (Table 3 and A6). Additionally, extreme ^{17}O-excess values of tap water did not always occur in the summer or winter either at the national or regional scale. Two possible reasons are that 1) tap water was not only from precipitation but from different water sources; 2) even for tap water that was mainly sourced from precipitation, the tap water isotopic signatures often lag behind precipitation (Zhao et al., 2017). It was noteworthy that the lowest $\delta'^{18}O$-$\delta'^{17}O$ slope of tap waters was observed in the summer from the NW region (0.5264) (Table 3). The low slope indicated that the tap waters in the summer might experience the evaporation effects over some arid and warm areas (Liu et al., 2009) or during storage and distribution (Good et al., 2014). The negative correlation between ^{17}O-excess and the summer temperature from the NW region indicated temperature had a contribution to the ^{17}O-excess variation of tap waters through kinetic fractionation associated with re-evaporation effect (Table A4). The re-evaporation effect is also supported by the negative correlation between $\delta^{18}O$ and summer precipitation amount (Table A4) through "amount effect" (Risi et al., 2008). At the same time, the low slope corresponded to the high ^{17}O-excess (42 per meg) possibly because 1) the water source itself has higher ^{17}O-excess value; 2) the continental recycling of moisture source is a main influencing factor as further discussed later on (e.g., in Urumqi of NW region).

4.2. Tap water as precipitation proxy

In theory precipitation ^{17}O-excess is mainly affected by RH (Barkan and Luz, 2005, 2007; Jacob and Sonntag, 1991) and the RH effect is supported by empirical observations. For instance, there are positive correlations between ^{17}O-excess and RH in Africa including monsoon rainfall and squall rainfall, influenced by strong re-evaporation processes (Landais et al., 2010). The

precipitation ^{17}O-excess is found to be correlated with the RH of the oceanic moisture source region on a subtropical island, revealing diffusional fractionation during evaporation in the ocean (Uechi and Uemura, 2019). At the same time, temperature can partially alter precipitation ^{17}O-excess. For example, for precipitation ^{17}O-excess in Switzerland, compared with RH (22%), higher R^2 of 60% and 36% is observed for the temperature of the moisture source site and the precipitation site, respectively (Affolter et al., 2015). The temperature effect might be because that evaporation is driven by RH (Craig and Gordon model) which is the ratio of partial vapor pressure and saturation vapor pressure. Saturation vapor pressure depends on temperature (Clausius-Clapeyron relation). Thus, changes in ^{17}O-excess due to evaporative processes could be caused by changes in either single factor or a combined factor of temperature and partial vapor pressure. When temperature increases, if partial vapor pressure stays constant, RH and thus ^{17}O-excess should decrease. Some other factors, other than RH and temperature at the source region and precipitation site, may contribute to the ^{17}O-excess variation, such as mixing of water vapor (origin of air masses and continental moisture recycling along air mass trajectories), convection and re-evaporation of precipitation (depending on re-evaporation rate and downdrafts intensity) (Landais et al., 2010; Li et al., 2015), and supersaturation process at low temperature (e.g., 0°C during liquid condensation of water vapor) (Deshpande et al., 2013). Therefore, to better identify the influencing factors of annual precipitation ^{17}O-excess at the national and regional scales, it is essential to address its sensitivity to environmental factors.

4.2.1. ^{17}O-excess variations at the national scale and the environmental controls

Precipitation in China are affected by both local climatic systems and Asian monsoons including southeast monsoon from the Pacific Ocean and southwest monsoon from the Indian Ocean (Araguás-Araguás et al., 1998; Liu et al., 2014; Vuille et al., 2005), resulting in large δ^{18}O

variations of precipitation across China (Zhao et al., 2012). The ^{17}O-excess mean value (40±5 per meg) of the 26 precipitation samples is similar to the global meteoric waters (35±16 per meg) (Table 4) (Li et al., 2015; Luz and Barkan, 2010). The mean value is higher than some other mid-latitude regions (e.g., Switzerland; 18 per meg) (Affolter et al., 2015) and the continental U.S. tap waters (most as precipitation; 17±11 per meg) (Li et al., 2015). But it is lower than that reported from Chicago in 2003-2005 (59 per meg) (Lin et al., 2013). The slope of precipitation $\delta'^{18}O$-$\delta'^{17}O$ (0.5292±0.0003) (Fig. 7) is close to that of GMWL (0.528) (Luz and Barkan, 2010). This indicated precipitation in China is mainly affected by the equilibrium fractionation effect at the annual scale. The effect of local environmental factors on annual precipitation isotope variations showed that precipitation ^{17}O-excess had weak negative correlation with altitude ($R^2 = 0.21$, $p = 0.02$). However, precipitation ^{17}O-excess had no correlation with the six environmental factors when three sites from the high altitude QP region (Lhasa, Nyingchi, and Gannan) were excluded, while $\delta^{18}O$ values were still correlated with four environmental factors (latitude, MAT, MAP, and MARH) (Table A5). These indicated that annual precipitation $\delta^{18}O$ variations are susceptible to the environmental factors especially the meteorological factors. However, precipitation ^{17}O-excess at the national scale does not correlate with the local environmental factors except in the QP region. The significant but weak altitude relationship for precipitation ^{17}O-excess across China is caused by the high altitude in the QP region.

A noteworthy finding was that the maximum and the minimum precipitation ^{17}O-excess values appeared simultaneously in the NE region (Heihe, 26 per meg; Changchun, 48 per meg). This is opposite to the similar $\delta^{18}O$ values in both sites exhibiting latitude effect (Liu et al., 2014), indicating that the ^{17}O-excess values contained additional information for the complexity of precipitation formation. The moisture source in Heihe might be mainly from the far away Arctic

ocean, similar to Qiqihar. Because the geographical location and altitude of Heihe (127.49° E, 50.24° N; 139 m) is close to Qiqihar (123.55° E, 47.23° N; 147 m), and Heihe has higher latitude and closer to the Arctic ocean, therefore Heihe precipitation is more susceptible to the Arctic ocean air masses (Araguás-Araguás et al., 1998). The MAT (2.0°C vs 4.3°C) and MAP (679 mm vs 581 mm) are also similar between the two cities (Table 4) (Araguás-Araguás et al., 1998). Based on these information, we think the lowest precipitation ^{17}O-excess in Heihe with the highest latitude in China was not caused by re-evaporation effect. This is because MAT in Heihe is very low (2.0°C) (Table 4). The temperature of lifting condensation level (i.e., cloud-base height) in Heihe has been calculated (-6.1°C) following the method from Barnes (1968). According to the Clausius-Clapeyron equation, the saturation vapor pressure decreases with decreasing temperature. Therefore, RH should increase if the partial vapor pressure stays constant while temperature is decreasing. This indicated the air could be supersaturated (i.e., partial vapor pressure exceeds saturation vapor pressure) when the temperature is low. Previous study also showed that the kinetic fractionation in super-saturated environment could occur at 0°C during liquid condensation of water vapor, similar to that reported for ice condensation (Deshpande et al., 2013). Additionally, most of the moisture in Heihe is from the Arctic ocean with cold air. Therefore, the lowest precipitation ^{17}O-excess in Heihe is possibly caused by kinetic fractionation associated with supersaturation process during the precipitation formation. As for Changchun (125.32° E, 43.89° N; 227 m), the moisture source might be from the north Pacific ocean, similar to Harbin (126.62° E, 45.68° N, 172 m) due to similar geographical locations as well as similar MAT and MAP (6.9°C vs 4.9°C; 521 mm vs 484 mm) between Changchun and Harbin (Table 4), and the former is even closer to the Pacific ocean (Araguás-Araguás et al., 1998). Therefore, compared with Heihe, snow and cold season rainfall in Changchun might experience more equilibrium fractionation processes

417 due to the higher temperature (6.9°C), and the shorter moisture transport from the Pacific ocean,
418 leading to the highest ^{17}O-excess value, similar to the northern U.S. (Li et al., 2015).

419 *4.2.2. Environmental control on ^{17}O-excess variations at the regional scale*

420 There are different climate regions and complex geographical conditions associated with
421 various climate characteristics throughout China. Previous study showed that moisture sources in
422 the N region are more complicated than other regions due to the geographical and meteorological
423 conditions (Liu et al., 2014). To address the geographical mismatch between natural water
424 resources and human demand, some large-scale hydraulic projects in China (e.g., Yangtze River
425 to Huai River, Luan River to Tianjin and Yellow River to Qingdao) have been constructed and the
426 major inter-basin transfer projects (e.g., South to North Water Transfer Project, from Yangtze
427 River to Yellow River and Hai River) are being implemented to alleviate water scarcity in the N
428 region (Crow-Miller, 2015; Moore, 2014; Piao et al., 2010). Additionally, some sites belong to
429 semiarid region (e.g., Longnan and Pingliang). Therefore, tap water was considered as
430 precipitation only for one site (Hanzhong) in the N region. The precipitation in Hanzhong was
431 strongly influenced by the East Asian summer monsoon (Kang et al., 1999; Tan et al., 2009). A
432 negative correlation between $\delta^{18}O$ of aragonite stalagmite and annual rainfall amount is found in
433 Hanzhong by Tan et al. (2009), indicating that the climatic control on isotopic compositions in
434 Hanzhong is similar to that in the SE region. Therefore, the precipitation ^{17}O-excess (42 per meg)
435 was close to those in the SE regions (Table 4).

436 The QP is the largest and highest plateau in the world and it provides the sources of the
437 Yangtze River and Yellow River. The boundary between the northern non-monsoon and southern
438 monsoon region affected by Indian ocean monsoon is approximately at 32°~33°N (Tanggula
439 Mountains) (Tian et al., 2001), resulting in different precipitation isotopes variations. The northern

non-monsoon region had higher ^{17}O-excess value (Gannan; 40 per meg) than those in the southern monsoon region (Lhasa and Nyingchi; 31 and 33 per meg) (Table 4). The moisture source of non-monsoon region precipitation (e.g., Delingha) originates from the dry continent due to being far away from the ocean and the block of Tanggula Mountains and has high d-excess value (Liu et al., 2008b). In our study, the d-excess value was also high in Gannan (13.1‰) along with high $\delta^{18}O$ value (-10.15‰) (Table 4). Therefore, the higher ^{17}O-excess value of precipitation in Gannan is likely influenced by recycled moisture. The moisture source of monsoon region precipitation (e.g., Lhasa) derives from the warm and humid Indian Ocean associated with low d-excess values (Liu et al., 2008b). In our study, the d-excess value was low in Lhasa (9.2‰) associated with low $\delta^{18}O$ value (-17.30‰) (Table 4). Therefore, the low ^{17}O-excess value in Lhasa is related to the high humidity from the Indian ocean. Additionally, due to the existence of glaciers nearby, the kinetic fractionation associated with supersaturation process at snow or glacier formation likely affects ^{17}O-excess of tap water in Lhasa (Jouzel et al., 2013; Pang et al., 2015).

The NW region is located in the hinterland of the Eurasia and to the north and northeast of the QP. It is classified as temperate continental arid climate (Liu et al., 2009). For Urumqi, the influence of south-western Indian oceanic current is small due to the obstruction of the QP, and the influence of south-eastern Pacific Oceanic current is weakened because of the long distance away from the ocean (Liu et al., 2009). Therefore, the westerly air currents and the local recycled water vapor are the main moisture sources in Urumqi (Kong et al., 2013; Pang et al., 2011; Tian et al., 2007; Zhao et al., 2019), and they are the dominant influencing factors lead to the high ^{17}O-excess value (43 per meg) (Table 4). Actually, the tap water in the Urumqi is also possibly supplied by meltwater due to the small $\delta^{18}O$ difference (0.14‰) between tap water and precipitation (Table

462 1) and previous study shows that Urumqi Glacier No.1 has lost mass over the past five decades
463 (1958~2008) to supply the regional water source (Li et al., 2007).

464 The number of precipitation proxy samples in the SE region accounted for half of the total
465 precipitation proxy samples (13/26). Most of the precipitation ^{17}O-excess values (36 to 47 per meg;
466 average 42±4 per meg) were higher than other regions, similar to the trend of high $\delta^{18}O$ values (-
467 5.18‰ to -8.06‰; average -6.67‰) (Table 4). No correlations were observed between ^{17}O-excess
468 and local environmental factors. Therefore, the higher ^{17}O-excess values in the SE region might
469 be caused by multiple factors including the moisture experiencing relatively short trajectories from
470 the evaporation origins to the precipitation sites (Liu et al., 2014), the greater local precipitation
471 amount (1136~2895 mm; 1838 mm) and higher RH (73.8%~82.3%; 77.6%) (Table 4).

472 The six precipitation proxy samples in the SW region were almost all located in the Yunnan-
473 Guizhou Plateau (eastern margin of the QP region) and still under Asian monsoon influence. The
474 range and mean value of annual precipitation ^{17}O-excess (33 to 42 per meg; 38±4 per meg) were
475 smaller and lower than those in the SE region, similar to the trend of $\delta^{18}O$ values (-7.24‰ to -
476 9.71‰, average -8.75‰) (Table 4). Specifically, the precipitation ^{17}O-excess in Tongren and Bose
477 were higher (42 and 41 per meg) with lower altitude (274 and 141 m) and higher precipitation
478 amount (1195 and 1450 mm), similar to the trend in the SE region. The other four sites (Baoshan,
479 Simao, Wenshan, and Bijie) had higher altitude (1268 to 1667 m) and a wide range of annual
480 precipitation amount (832 to 1482 mm) (Table 4). For Simao and Wenshan, the precipitation might
481 be affected by re-evaporation because of the observed low d-excess values (7.1‰ and 7.7‰),
482 leading to low ^{17}O-excess values (36 and 33 per meg) (Table 4).

483

5. CONCLUSIONS

This is the first study on the ^{17}O-excess variations of tap waters across China. The result showed that the annual ^{17}O-excess variations of the tap waters (92 sites) varied between 26 and 55 per meg with a mean value of 39±5 per meg. The tap water ^{17}O-excess values did not show obvious spatial pattern, and were almost unaffected by local environmental factors except in the QP region with a strong latitudinal relationship. The mean ^{17}O-excess values in different seasons (38 to 40 per meg) were not significantly different at the national scale nor in different regions. Most of the tap water ^{17}O-excess variations in the six climate regions were likely influenced by the equilibrium fractionation effect both at the annual and seasonal scale, except for NW region in the summer. The tap water ^{17}O-excess variations in the NW region were influenced by kinetic fractionation associated with re-evaporation effect.

To evaluate the spatial characteristics of precipitation ^{17}O-excess, tap water from 26 sites were used as precipitation proxy. These sites include reported surface water-dominated sites with humid climate (aridity index >0.5) and sites with small $\delta^{18}O$ differences (<0.5‰) between local precipitation and tap water. It is worth noting that compared with the obvious spatial characteristics of $\delta^{18}O$, ^{17}O-excess of precipitation-sourced tap water did not show spatial trend. But ^{17}O-excess variations of precipitation-sourced tap water revealed much detailed precipitation formation mechanisms. For example, kinetic fractionation associated with supersaturation process in snow or glacier formation was responsible for the low ^{17}O-excess variations in the NE (Heihe) and QP southern monsoon regions (Lhasa). Re-evaporation effect also played an important role for low ^{17}O-excess variations such as in Simao and Wenshan. However, in the inland, far away from the ocean and with the blocking effect of mountains, continent recycled moisture was responsible for the high ^{17}O-excess values in local precipitation, such as in Gannan in the non-monsoon QP region,

and in Urumqi in the NW arid region. In the SE region, higher ^{17}O-excess variation might be caused by multiple factors including moisture experiencing relatively short trajectories from the evaporation origins to the precipitation sites, greater local precipitation amount and higher RH. Overall, the ^{17}O-excess variations preserve valuable information to reveal the precipitation formation mechanisms across China.

ACKNOWLEDGEMENTS

We thank the contributions of three anonymous reviewers, executive editor Professor Jeffrey Catalano and associate editor Professor Orit Sivan. Their constructive comments and suggestions helped us significantly improve the quality of the manuscript. Funding for this work was made available from the Indiana University-Purdue University Indianapolis Research Support Funds Grant, the President's International Research Awards from Indiana University and U.S. National Science Foundation (EAR-1554894).

REFERENCES

Affolter, S., Häuselmann, A.D., Fleitmann, D., Häuselmann, P. and Leuenberger, M. (2015) Triple isotope (δD, $\delta^{17}O$, $\delta^{18}O$) study on precipitation, drip water and speleothem fluid inclusions for a Western Central European cave (NW Switzerland). *Quat. Sci. Rev.* **127**, 73-89.

Angert, A., Cappa, C.D. and DePaolo, D.J. (2004) Kinetic ^{17}O effects in the hydrologic cycle: Indirect evidence and implications. *Geochim. Cosmochim. Acta* **68**, 3487-3495.

Araguás-Araguás, L., Froehlich, K. and Rozanski, K. (1998) Stable isotope composition of precipitation over southeast Asia. *J. Geophys. Res.* **103**, 28721-28742.

Barkan, E. and Luz, B. (2005) High precision measurements of $^{17}O/^{16}O$ and $^{18}O/^{16}O$ ratios in H_2O. *Rapid Commun. Mass Spectrom.* **19**, 3737-3742.

Barkan, E. and Luz, B. (2007) Diffusivity fractionations of $H_2{}^{16}O/H_2{}^{17}O$ and $H_2{}^{16}O/H_2{}^{18}O$ in air and their implications for isotope hydrology. *Rapid Commun. Mass Spectrom.* **21**, 2999-3005.

Barnes, S.L. (1968) An empirical shortcut to the calculation of temperature and pressure at the lifted condensation level. *Journal of Applied Meteorology* **7**, 511-511.

Berman, E.S., Levin, N.E., Landais, A., Li, S. and Owano, T. (2013) Measurement of $\delta^{18}O$, $\delta^{17}O$ and ^{17}O-excess in water by Off-Axis Integrated Cavity Output Spectroscopy and Isotope Ratio Mass Spectrometry. *Anal. Chem.* **85**, 10392-10398.

Chen, Z., Cheng, J., Guo, P., Lin, z. and Zhang, F. (2010) Distribution characters and its control factors of stable isotope in precipitation over China. *Transactions of Atmospheric Sciences* **33**, 667-679.

Crow-Miller, B. (2015) Discourses of deflection: the politics of framing China's south-north water transfer project. *Water Altern.* **8**, 173-192.

Dansgaard, W. (1964) Stable isotopes in precipitation. *Tellus* **16**, 436-468.

Deshpande, R., Maurya, A., Kumar, B., Sarkar, A. and Gupta, S. (2013) Kinetic fractionation of water isotopes during liquid condensation under super-saturated condition. *Geochim. Cosmochim. Acta* **100**, 60-72.

Gohari, A., Eslamian, S., Mirchi, A., Abedi-Koupaei, J., Bavani, A.M. and Madani, K. (2013) Water transfer as a solution to water shortage: A fix that can backfire. *J. Hydrol.* **491**, 23-39.

Good, S.P., Kennedy, C.D., Stalker, J.C., Chesson, L.A., Valenzuela, L.O., Beasley, M.M., Ehleringer, J.R. and Bowen, G. (2014) Patterns of local and nonlocal water resource use across the western U.S. determined via stable isotope intercomparisons. *Water Resour. Res.* **50**, 8034-8049.

Jacob, H. and Sonntag, C. (1991) An 8-year record of the seasonal variation of ^{2}H and ^{18}O in atmospheric water vapour and precipitation at Heidelberg, Germany. *Tellus B* **43**, 291-300.

Jameel, Y., Brewer, S., Good, S.P., Tipple, B.J., Ehleringer, J.R. and Bowen, G.J. (2016) Tap water isotope ratios reflect urban water system structure and dynamics across a semiarid metropolitan area. *Water Resour. Res.* **52**, 5891-5910.

Johnson, K.R. and Ingram, B.L. (2004) Spatial and temporal variability in the stable isotope systematics of modern precipitation in China: implications for paleoclimate reconstructions. *Earth Planet. Sci. Lett.* **220**, 365-377.

Jouzel, J., Delaygue, G., Landais, A., Masson-Delmotte, V., Risi, C. and Vimeux, F. (2013) Water isotopes as tools to document oceanic sources of precipitation. *Water Resour. Res.* **49**, 7469-7486.

Kang, I.-S., Ho, C.-H., Lim, Y.-K. and Lau, K. (1999) Principal modes of climatological seasonal and intraseasonal variations of the Asian summer monsoon. *Monthly weather review* **127**, 322-340.

Katsuyama, M., Yoshioka, T. and Konohira, E. (2015) Spatial distribution of oxygen-18 and deuterium in stream waters across the Japanese archipelago. *Hydrol. Earth Syst. Sc.* **19**, 1577-1588.

Kong, Y., Pang, Z. and Froehlich, K. (2013) Quantifying recycled moisture fraction in precipitation of an arid region using deuterium excess. *Tellus B* **65**, 19251.

569 Lachniet, M.S. and Patterson, W.P. (2009) Oxygen isotope values of precipitation and surface waters in
570 northern Central America (Belize and Guatemala) are dominated by temperature and amount
571 effects. *Earth Planet. Sci. Lett.* **284**, 435-446.
572 Landais, A., Ekaykin, A., Barkan, E., Winkler, R. and Luz, B. (2012a) Seasonal variations of ^{17}O-excess and
573 d-excess in snow precipitation at Vostok station, East Antarctica. *J. Glaciol.* **58**, 725-733.
574 Landais, A., Risi, C., Bony, S., Vimeux, F., Descroix, L., Falourd, S. and Bouygues, A. (2010) Combined
575 measurements of ^{17}O-excess and d-excess in African monsoon precipitation: Implications for
576 evaluating convective parameterizations. *Earth Planet. Sci. Lett.* **298**, 104-112.
577 Landais, A., Steen-Larsen, H.C., Guillevic, M., Masson-Delmotte, V., Vinther, B. and Winkler, R. (2012b)
578 Triple isotopic composition of oxygen in surface snow and water vapor at NEEM (Greenland).
579 *Geochim. Cosmochim. Acta* **77**, 304-316.
580 Li, S., Levin, N.E. and Chesson, L.A. (2015) Continental scale variation in ^{17}O-excess of meteoric waters in
581 the United States. *Geochim. Cosmochim. Acta* **164**, 110-126.
582 Li, S., Levin, N.E., Soderberg, K., Dennis, K.J. and Caylor, K.K. (2017) Triple oxygen isotope composition of
583 leaf waters in Mpala, central Kenya. *Earth Planet. Sci. Lett.* **468**, 38-50.
584 Li, X., Zhang, M., Li, Y., Wang, S., Huang, X., Ma, Q. and Ma, X. (2012) Characteristics of $\delta^{18}O$ in
585 Precipitation and Moisture Transports over the Arid Region in Northwest China. *Environmental*
586 *Science* **33**, 711-719.
587 Li, Z., Shen, Y., Wang, F., Li, H., Dong, Z., Wang, W. and Wang, L. (2007) Response of glacier melting to
588 climate change-take Urumqi Glacier No. 1 as an example. *J. Glaciol. Geocryol.* **29**, 333-342.
589 Lin, Y., Clayton, R.N., Huang, L., Nakamura, N. and Lyons, J.R. (2013) Oxygen isotope anomaly observed
590 in water vapor from Alert, Canada and the implication for the stratosphere. *Proc. Natl. Acad. Sci.*
591 **110**, 15608-15613.
592 Liu, J., Song, X., Sun, X., Yuan, G., Liu, X. and Wang, S. (2009) Isotopic composition of precipitation over
593 Arid Northwestern China and its implications for the water vapor origin. *J. Geogr. Sci.* **19**, 164-174.
594 Liu, J., Song, X., Yuan, G., Sun, X., Liu, X., Chen, F., Wang, Z. and Wang, S. (2008a) Characteristics of $\delta^{18}O$
595 in Precipitation over Northwest China and Its Water Vapor Sources. *Acta Geographica Sinica* **63**.
596 Liu, J., Song, X., Yuan, G., Sun, X. and Yang, L. (2014) Stable isotopic compositions of precipitation in
597 China. *Tellus B* **66**, 22567.
598 Liu, Z., Tian, L., Yao, T. and Yu, W. (2008b) Seasonal deuterium excess in Nagqu precipitation: influence
599 of moisture transport and recycling in the middle of Tibetan Plateau. *Environmental Geology* **55**,
600 1501-1506.
601 Luz, B. and Barkan, E. (2010) Variations of $^{17}O/^{16}O$ and $^{18}O/^{16}O$ in meteoric waters. *Geochim. Cosmochim.*
602 *Acta* **74**, 6276-6286.
603 McDonald, R.I., Green, P., Balk, D., Fekete, B.M., Revenga, C., Todd, M. and Montgomery, M. (2011)
604 Urban growth, climate change, and freshwater availability. *Proc. Natl. Acad. Sci.* **108**, 6312-6317.
605 Meijer, H. and Li, W. (1998) The use of electrolysis for accurate $\delta^{17}O$ and $\delta^{18}O$ isotope measurements in
606 water. *Isotopes Environ. Health Studies* **34**, 349-369.
607 Moore, S.M. (2014) Modernisation, authoritarianism, and the environment: the politics of China's
608 South-North Water Transfer Project. *Env. Polit.* **23**, 947-964.
609 Nickum, J.E. (1998) Is China living on the water margin? *The China Quarterly* **156**, 880-898.
610 Pang, H., Hou, S., Landais, A., Masson-Delmotte, V., Prie, F., Steen-Larsen, H.C., Risi, C., Li, Y., Jouzel, J.
611 and Wang, Y. (2015) Spatial distribution of ^{17}O-excess in surface snow along a traverse from
612 Zhongshan station to Dome A, East Antarctica. *Earth Planet. Sci. Lett.* **414**, 126-133.
613 Pang, Z., Kong, Y., Froehlich, K., Huang, T., Yuan, L., Li, Z. and Wang, F. (2011) Processes affecting
614 isotopes in precipitation of an arid region. *Tellus B* **63**, 352-359.
615 Pekel, J.-F., Cottam, A., Gorelick, N. and Belward, A.S. (2016) High-resolution mapping of global surface
616 water and its long-term changes. *Nature* **540**, 418-422.

Piao, S., Ciais, P., Huang, Y., Shen, Z., Peng, S., Li, J., Zhou, L., Liu, H., Ma, Y. and Ding, Y. (2010) The impacts of climate change on water resources and agriculture in China. *Nature* **467**, 43-51.

Risi, C., Bony, S. and Vimeux, F. (2008) Influence of convective processes on the isotopic composition ($\delta^{18}O$ and δD) of precipitation and water vapor in the tropics: 2. Physical interpretation of the amount effect. *J. Geophys. Res.* **113**.

Rozanski, K., Araguás‐Araguás, L. and Gonfiantini, R. (1993) Isotopic patterns in modern global precipitation. *Climate change in continental isotopic records* **78**, 1-36.

Schoenemann, S.W., Schauer, A.J. and Steig, E.J. (2013) Measurement of SLAP2 and GISP $\delta^{17}O$ and proposed VSMOW-SLAP normalization for $\delta^{17}O$ and ^{17}O-excess. *Rapid Commun. Mass Spectrom.* **27**, 582-590.

Schoenemann, S.W., Steig, E.J., Ding, Q., Markle, B.R. and Schauer, A.J. (2014) Triple water-isotopologue record from WAIS Divide, Antarctica: Controls on glacial-interglacial changes in ^{17}O-excess of precipitation. *J. Geophys. Res.* **119**, 8741-8763.

Steig, E., Gkinis, V., Schauer, A., Schoenemann, S., Samek, K., Hoffnagle, J., Dennis, K. and Tan, S. (2014) Calibrated high-precision ^{17}O-excess measurements using cavity ring-down spectroscopy with laser-current-tuned cavity resonance. *Atmos. Meas. Tech.* **7**, 2421-2435.

Tan, L., Cai, Y., Cheng, H., An, Z. and Edwards, R.L. (2009) Summer monsoon precipitation variations in central China over the past 750 years derived from a high-resolution absolute-dated stalagmite. *Palaeogeography, Palaeoclimatology, Palaeoecology* **280**, 432-439.

Tian, C. and Wang, L. (2019) Stable isotope variations of daily precipitation from 2014-2018 in the central United States. *Scientific Data* **6**, 190018.

Tian, C., Wang, L., Kaseke, K.F. and Bird, B.W. (2018) Stable isotope compositions ($\delta^{2}H$, $\delta^{18}O$ and $\delta^{17}O$) of rainfall and snowfall in the central United States. *Sci. Rep.* **8**, 6712.

Tian, C., Wang, L. and Novick, K.A. (2016) Water vapor $\delta^{2}H$, $\delta^{18}O$ and $\delta^{17}O$ measurements using an off-axis integrated cavity output spectrometer-sensitivity to water vapor concentration, delta value and averaging-time. *Rapid Commun. Mass Spectrom.* **30**, 2077-2086.

Tian, L., Yao, T., MacClune, K., White, J., Schilla, A., Vaughn, B., Vachon, R. and Ichiyanagi, K. (2007) Stable isotopic variations in west China: A consideration of moisture sources. *J. Geophys. Res.* **112**.

Tian, L., Yao, T., Sun, W., Stievenard, M. and Jouzel, J. (2001) Relationship between δD and $\delta^{18}O$ in precipitation on north and south of the Tibetan Plateau and moisture recycling. *Science in China Series D: Earth Sciences* **44**, 789-796.

Uechi, Y. and Uemura, R. (2019) Dominant influence of the humidity in the moisture source region on the 17O-excess in precipitation on a subtropical island. *Earth Planet. Sci. Lett.* **513**, 20-28.

Uemura, R., Barkan, E., Abe, O. and Luz, B. (2010) Triple isotope composition of oxygen in atmospheric water vapor. *Geophys. Res. Lett.* **37**.

Van Hook, W.A. (1968) Vapor pressures of the isotopic waters and ices. *J. Phys. Chem.* **72**, 1234-1244.

Vuille, M., Werner, M., Bradley, R. and Keimig, F. (2005) Stable isotopes in precipitation in the Asian monsoon region. *J. Geophys. Res.* **110**.

Wang, L., Caylor, K.K. and Dragoni, D. (2009) On the calibration of continuous, high-precision $\delta^{18}O$ and $\delta^{2}H$ measurements using an off-axis integrated cavity output spectrometer. *Rapid Commun. Mass Spectrom.* **23**, 530-536.

Wang, L., Caylor, K.K., Villegas, J.C., Barron-Gafford, G.A., Breshears, D.D. and Huxman, T.E. (2010) Partitioning evapotranspiration across gradients of woody plant cover: Assessment of a stable isotope technique. *Geophys. Res. Lett.* **37**.

West, A., February, E. and Bowen, G. (2014) Spatial analysis of hydrogen and oxygen stable isotopes ("isoscapes") in ground water and tap water across South Africa. *J. Geochem. Explor.* **145**, 213-222.

Winkler, R., Landais, A., Sodemann, H., Dümbgen, L., Prié, F., Masson-Delmotte, V., Stenni, B. and Jouzel, J. (2012) Deglaciation records of ^{17}O-excess in East Antarctica: reliable reconstruction of oceanic normalized relative humidity from coastal sites. *Clim. Past* **8**, 1-16.

Xie, F., Yu, Y.-L. and Qin, X.-N. (2015) NCEP Reanalysis and Precipitation Isotopes to Discuss Water Vapor Source in Baotou, 2015 6th International Conference on Manufacturing Science and Engineering. Atlantis Press.

Xie, L., Wei, G., Deng, W. and Zhao, X. (2011) Daily δ18O and δD of precipitations from 2007 to 2009 in Guangzhou, South China: Implications for changes of moisture sources. *J. Hydrol.* **400**, 477-489.

Xu, J. (2013) Study on the difference of precipitation annual distribution in Baoshan district of Yunnan province. *Journal of Baoshan Teachers' College* **32**, 22-25.

Yu, W., Yao, T., Lewis, S., Tian, L., Ma, Y., Xu, B. and Qu, D. (2014) Stable oxygen isotope differences between the areas to the north and south of Qinling Mountains in China reveal different moisture sources. *International Journal of Climatology* **34**, 1760-1772.

Yu, W., Yao, T., Tian, L., Ma, Y., Wen, R., Devkota, L.P., Wang, W., Qu, D. and Chhetri, T.B. (2016) Short-term variability in the dates of the Indian monsoon onset and retreat on the southern and northern slopes of the central Himalayas as determined by precipitation stable isotopes. *Clim. Dyn.* **47**, 159-172.

Yu, Y., Zhang, Q., Chen, T., Zhao, J. and Han, H. (2006) Analysis on the potential precipitation resources over East Gansu. *Journal of Meteorological Research* **20**, 60-68.

Zhang, X.P., Liu, J.M., Wang, X.Y., Nakawo, M., Xie, Z.C., Zhang, J.M. and Zhang, X.Z. (2010) Climatological significance of stable isotopes in precipitation over south‐west China. *International Journal of Climatology* **30**, 2229-2239.

Zhao, L., Liu, X., Wang, N., Kong, Y., Song, Y., He, Z., Liu, Q. and Wang, L. (2019) Contribution of recycled moisture to local precipitation in the inland Heihe River Basin. *Agricultural and Forest Meteorology* **271**, 316-335.

Zhao, L., Xiao, H., Zhou, M., Cheng, G., Wang, L., Yin, L. and Ren, J. (2012) Factors controlling spatial and seasonal distributions of precipitation $\delta^{18}O$ in China. *Hydrol. Process.* **26**, 143-152.

Zhao, S., Hu, H., Tian, F., Tie, Q., Wang, L., Liu, Y. and Shi, C. (2017) Divergence of stable isotopes in tap water across China. *Sci. Rep.* **7**, 43653.

Declarations of interest: none

699 **Table 1 Summary of mean annual $\delta^{18}O$ values of reference precipitation as well as the**
700 **mean annual $\delta^{18}O$ and ^{17}O-excess of the observed tap water samples as precipitation proxy.**

City	Region	Reference values	Observed values	
		$\delta^{18}O$ (‰)	$\delta^{18}O$ (‰)	^{17}O-excess (per meg)
Urumqi	NW	-10.84[a]	-10.70	43
Lhasa	QP	-17.16[b]	-17.30	31
Changsha	SE	-5.65[a]	-5.18	45
Guilin	SE	-6.13[a]	-6.32	41
Fuzhou	SE	-6.40[a]	-6.56	41
Liuzhou	SE	-6.43[a]	-6.17	36
Guangzhou	SE	-5.90[a]	-5.99	47
Haikou	SE	-6.62[a]	-6.60	44

701

702 **Noting: a was from Araguás-Araguás, L. and Froehlich, K. (1998); b was from Johnson, KR. (2004)**

703
704
705
706
707
708
709
710
711
712
713
714
715
716
717
718

719 **Table 2 The range and mean values of ^{17}O-excess variations, geographical and meteorological variables for annual tap waters**
720 **in six different geographical zones. N, NE, NW, QP, SE, and SW was northern, northeastern, northwestern, Qinghai-Tibet**
721 **Plateau, southeastern, and southwestern, respectively. Numbers in the parentheses are mean annual values, and mean values ±**
722 **stand deviation for ^{17}O-excess variations.**

Region	^{17}O-excess (per meg)	Longitude (°)	Latitude (°)	Altitude (m)	Temperature (°C)	Precipitation (mm)	Relative Humidity (%)	Sample number (n)
N	33~48 (39±4)	103.75~121.38	33.08~42.27	5~1905 (503)	7.4~15.9 (12.7)	189~925 (539)	47.1~75.6 (60.2)	28
NE	26~48 (35±7)	121.60~127.49	38.92~50.24	18~273 (132)	2.0~12.0 (7.5)	414~909 (573)	47.6~67.9 (60.1)	8
NW	32~47 (40±5)	75.99~116.07	38.47~45.6	410~1470 (1034)	3.5~13.2 (8.9)	60~586 (214)	41.6~59.7 (49.0)	11
QP	31~43 (38±5)	91.13~102.51	29.58~37.37	2261~3657 (3006)	3.6~9.5 (6.8)	73~934 (388)	30.4~62.9 (46.7)	6
SE	34~55 (42±5)	108.31~121.47	20.03~33.39	5~421 (74)	15.1~25.1 (19.1)	1136~2895 (1667)	71.2~83.2 (77.3)	26
SW	30~43 (38±4)	99.17~109.19	22.80~30.66	141~1907 (1100)	13.9~22.6 (17.7)	832~1482 (1154)	56.6~83.1 (73.0)	13
All	26~55 (39±5)	75.99~127.49	20.03~50.24	5~3657 (660)	2.0~25.1 (13.9)	60~2895 (899)	30.4~83.2 (64.6)	92

724 **Table 3 ^{17}O-excess mean values and the slopes between δ′^{18}O-δ′^{17}O in different seasons and**
725 **six geographical zones for tap water samples.**

	Winter			Spring			Summer			Fall		
Regions	^{17}O-excess (per meg)	Slope	n	^{17}O-excess (per meg)	Slope	n	^{17}O-excess (per meg)	Slope	n	^{17}O-excess (per meg)	Slope	n
N	40±8	0.5290	22	38±5	0.5293	27	39±6	0.5281	21	39±5	0.5286	20
NE	37±7	0.5280	6	31±8	0.5277	7	33±8	0.5299	6	35±7	0.5298	6
NW	35±7	0.5294	9	42±4	0.5296	9	42±6	0.5264	5	37±5	0.5279	4
QP	35±7	0.5290	6	36±4	0.5285	6	41±7	0.5301	6	38±5	0.5294	6
SE	45±6	0.5292	21	42±6	0.5283	25	41±4	0.5289	17	42±4	0.5296	16
SW	38±8	0.5284	11	37±5	0.5291	13	37±5	0.5294	11	40±3	0.5285	11
All	40±8	0.5294	75	38±6	0.5289	87	38±6	0.5288	66	39±5	0.5291	63

726

727

728 **Table 4 The geographical and meteorological information, as well as the annual ^{17}O-excess, $\delta^{18}O$, and d-excess values of 26**
729 **precipitation-sourced samples.**
730

City	Region	^{17}O-excess (per meg)	$\delta^{18}O$ (‰)	d-excess (‰)	Longitude (°)	Latitude (°)	Altitude (m)	Temperature (°C)	Precipitation (mm)	Relative Humidity (%)	Main moisture source
Heihe	NE	26	-14.45	8.7	127.49	50.24	139	2.0	679	66.2	NA
Changchun	NE	48	-10.36	2.9	125.32	43.89	227	6.9	521	59.8	NA
Hanzhong	N	42	-8.43	12.9	107.03	33.08	515	15.8	839	75.6	Western pacific (Kang et al., 1999; Tan et al., 200
Gannan	QP	40	-10.15	13.1	102.51	35.20	3012	3.6	447	62.9	NA
Lhasa	QP	31	-17.30	9.2	91.13	29.66	3657	9.5	340	34.3	Indian Ocean (Liu et al., 2008b)
Nyingchi	QP	33	-13.81	12.1	94.48	29.58	3300	9.5	934	62.7	NA
Urumqi	NW	43	-10.70	13.0	87.61	43.79	883	3.5	586	59.7	Advected moisture of westerlies and local recycled moisture (Kong et al., 2013; Pang et al., 2011; Tian et al., 2007)
Enshi	SE	46	-7.37	12.3	109.48	30.27	421	17.2	1193	78.1	NA
Nantong	SE	36	-7.09	10.3	120.86	32.02	11	15.8	1705	76.6	NA
Quzhou	SE	40	-6.76	12.2	118.87	28.96	79	17.8	2446	80.4	NA
Lishui	SE	42	-7.37	12.6	119.92	28.45	64	18.9	1523	74.0	NA
Fuzhou	SE	41	-6.56	11.8	119.30	26.08	18	20.5	1655	73.8	South pacific (Araguás-Araguás et al., 1998)
Longyan	SE	46	-6.59	13.6	117.03	25.11	365	20.7	1975	75.3	NA
Shaoguan	SE	45	-6.60	13.6	113.61	24.81	65	20.7	1954	80.0	NA
Nanning	SE	42	-8.06	8.8	108.31	22.81	80	22.1	1136	82.3	NA
Changsha	SE	45	-5.18	11.4	112.98	28.20	54	17.5	1453	79.9	South pacific (Araguás-Araguás et al., 1998)
Guilin	SE	41	-6.32	13.4	110.29	25.28	160	19.9	2895	74.8	South pacific (Araguás-Araguás et al., 1998)
Liuzhou	SE	36	-6.17	14.1	109.40	24.31	65	21.5	1889	74.9	South pacific (Araguás-Araguás et al., 1998; Yu et al., 2014)
Guangzhou	SE	47	-5.99	10.7	113.26	23.12	28	22.1	2424	77.2	South pacific (Araguás-Araguás et al., 1998)
Haikou	SE	44	-6.60	8.2	110.35	20.03	15	25.1	1646	81.2	South pacific (Araguás-Araguás et al., 1998; Yu et al., 2014)

Tongren	**SW**	**42**	**-7.24**	**14.4**	**109.19**	**27.72**	**274**	**17.4**	**1195**	**77.1**	**NA**
Bose	**SW**	**41**	**-8.91**	**11.0**	**106.61**	**23.90**	**141**	**22.6**	**1450**	**76.7**	**NA**
Baoshan	**SW**	**40**	**-9.71**	**9.2**	**99.17**	**25.12**	**1667**	**17.3**	**832**	**66.0**	**Indian Ocean (Xu, 2013)**
Simao	**SW**	**36**	**-8.70**	**7.1**	**100.98**	**22.80**	**1336**	**19.5**	**1482**	**76.1**	**NA**
Wenshan	**SW**	**33**	**-9.07**	**7.7**	**104.24**	**23.37**	**1268**	**18.6**	**1103**	**78.0**	**NA**
Bijie	**SW**	**39**	**-8.87**	**11.8**	**105.28**	**27.31**	**1478**	**13.9**	**1044**	**81.3**	**NA**

731

732

733

734

735

736

737

738

739

740

741

742

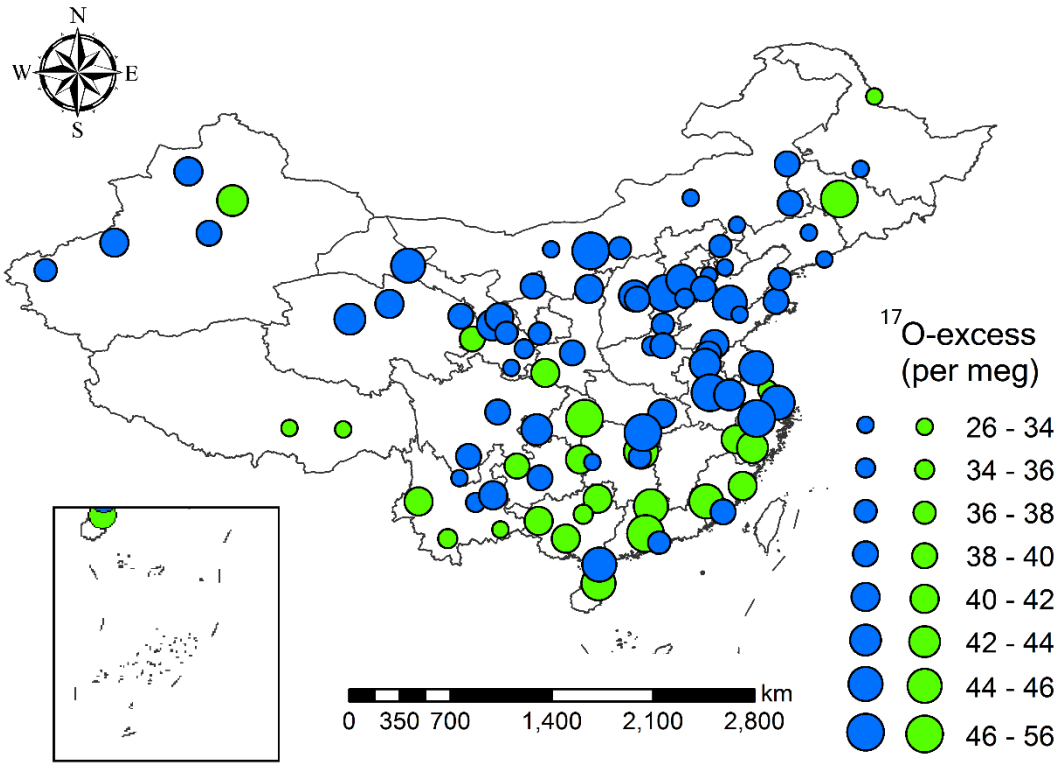

743

744 **Fig. 1 Summary of ^{17}O-excess annual values for different types of tap water samples in**
745 **China. Green circle represents 26 tap water from precipitation sources, blue circle**
746 **represents tap water likely from other sources.**

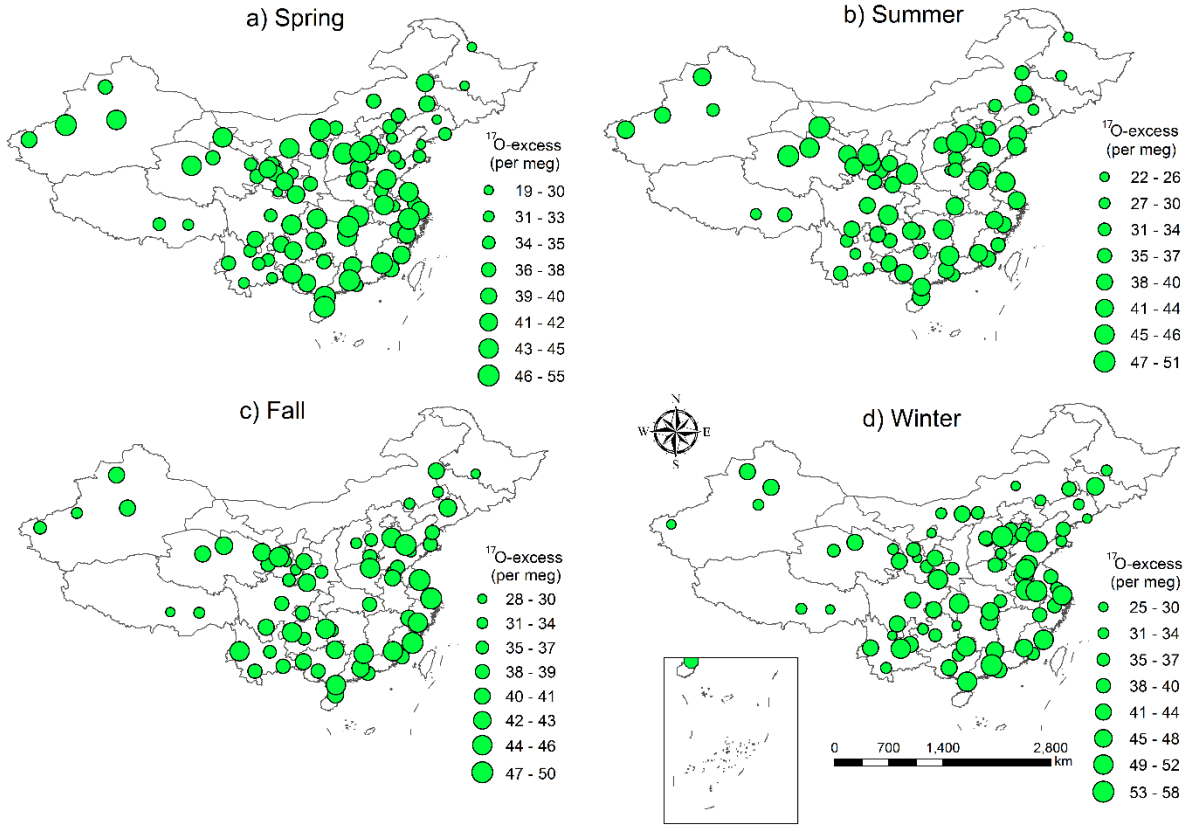

747
748 **Fig. 2 Summary of ^{17}O-excess values of tap water samples in different seasons.**

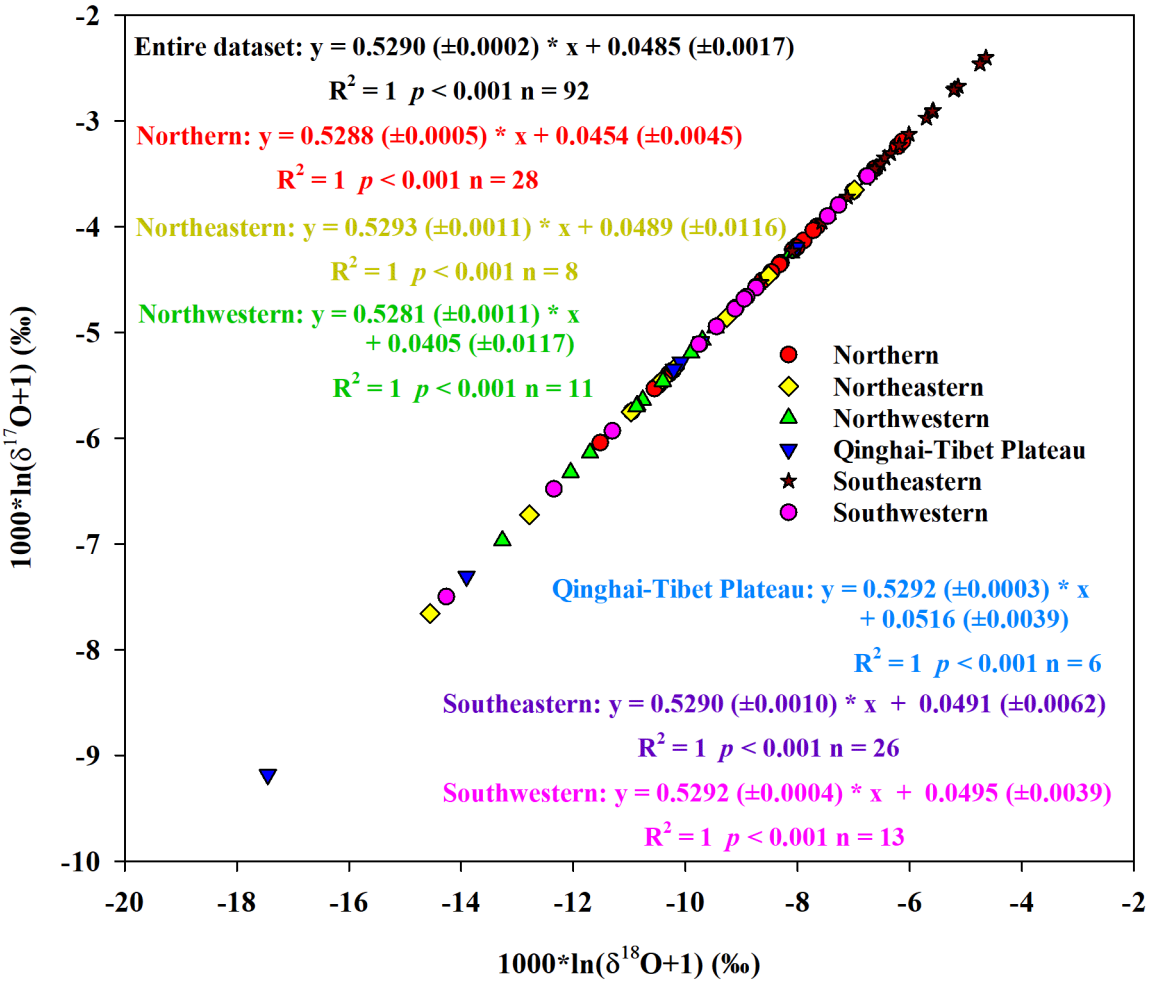

Fig. 3 Annual tap water $\delta'^{18}O$ and $\delta'^{17}O$ relationships at the national-scale and in six different geographical zones.

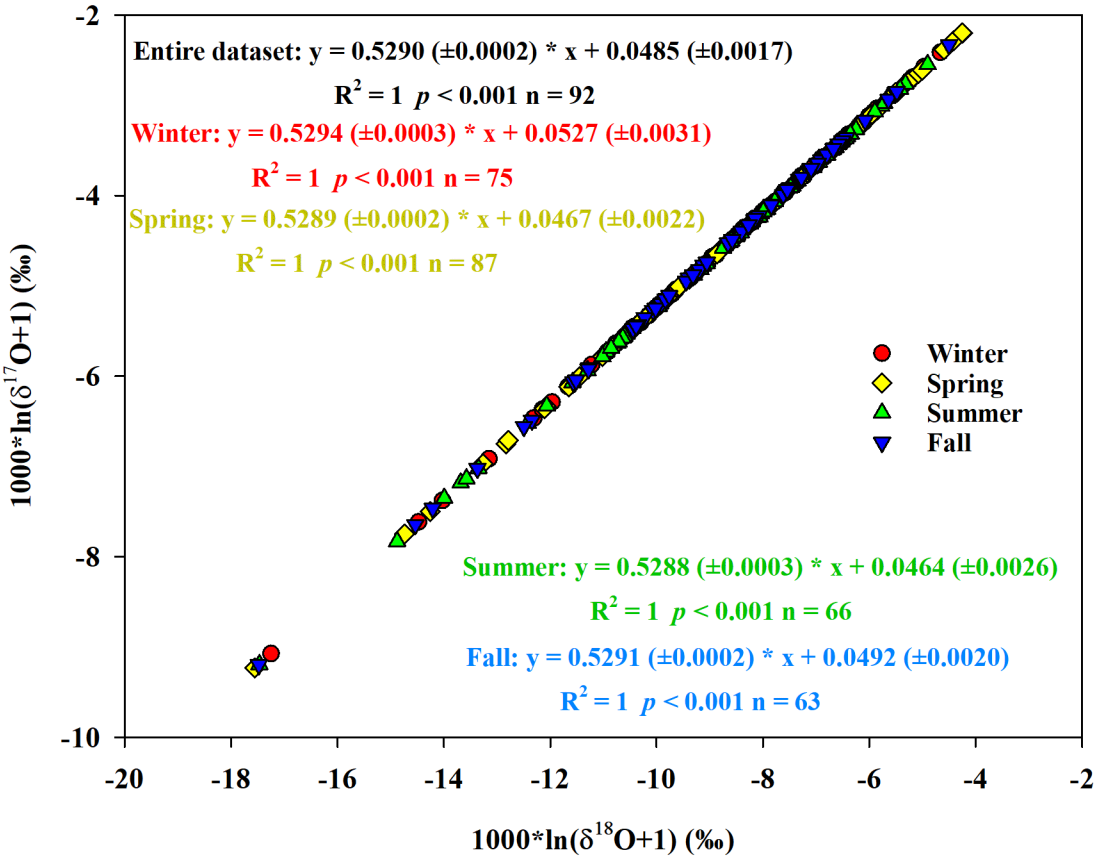

753

754 **Fig. 4 The relationships between tap water δ′^{18}O and δ′^{17}O in different seasons.**

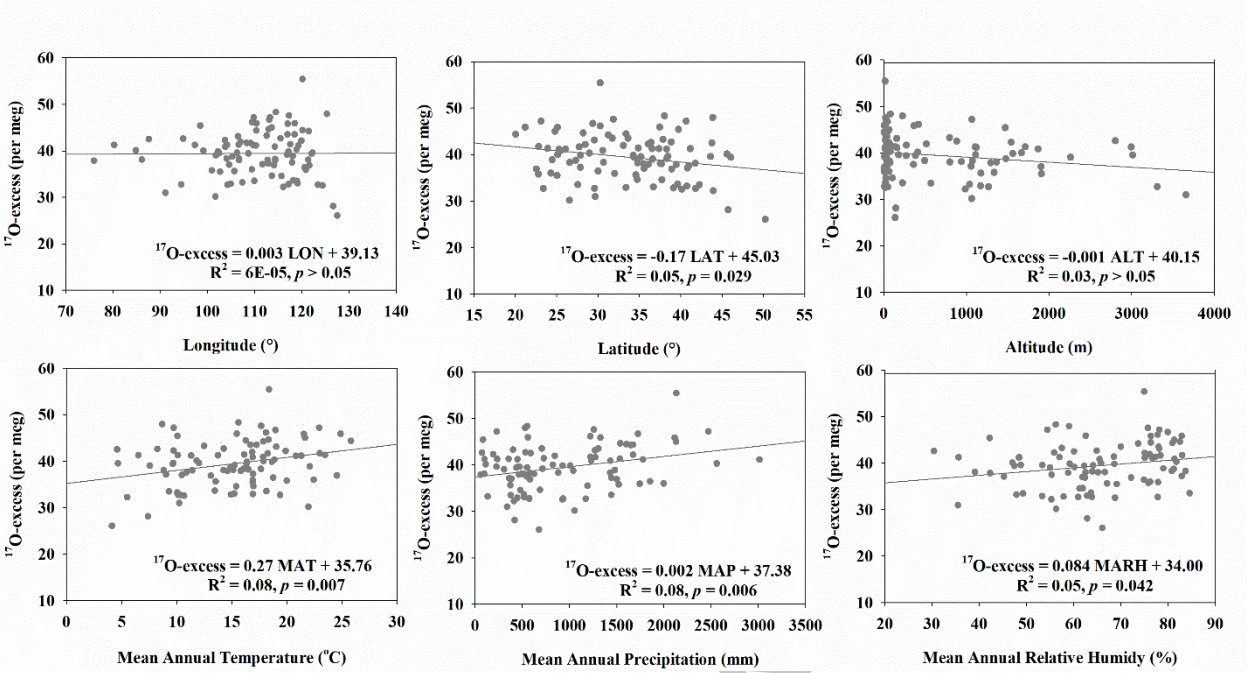

Fig. 5 The relationships between mean annual ^{17}O-excess values and environmental factors for tap water at the national scale.

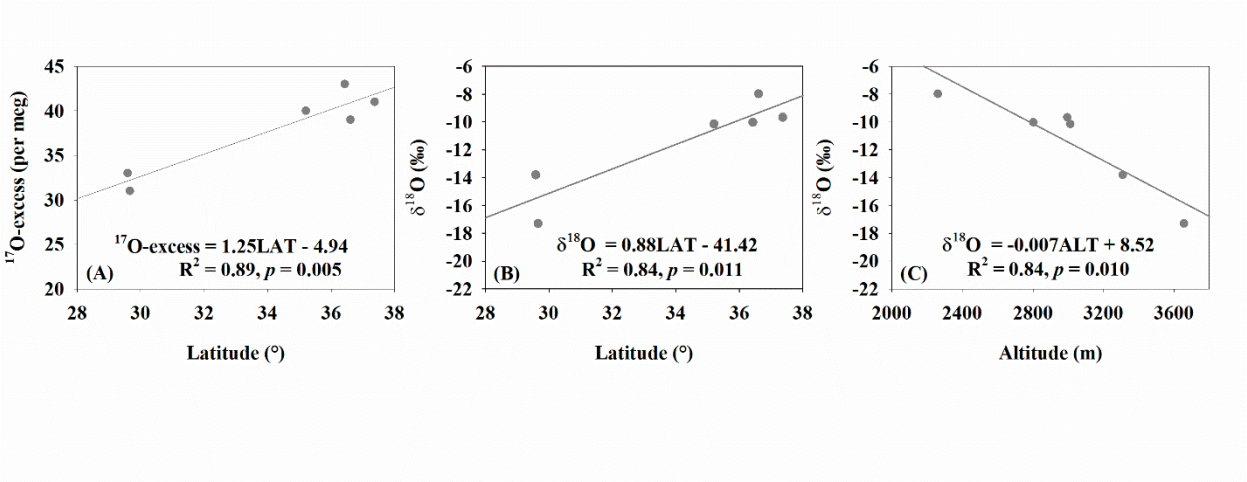

759

760 **Fig. 6 The relationships between mean annual ^{17}O-excess values and the latitude (A), as**
761 **well as between the δ^{18}O values and the latitude (B) and altitude (C) for tap water in the**
762 **Qinghai-Tibet Plateau region.**

763

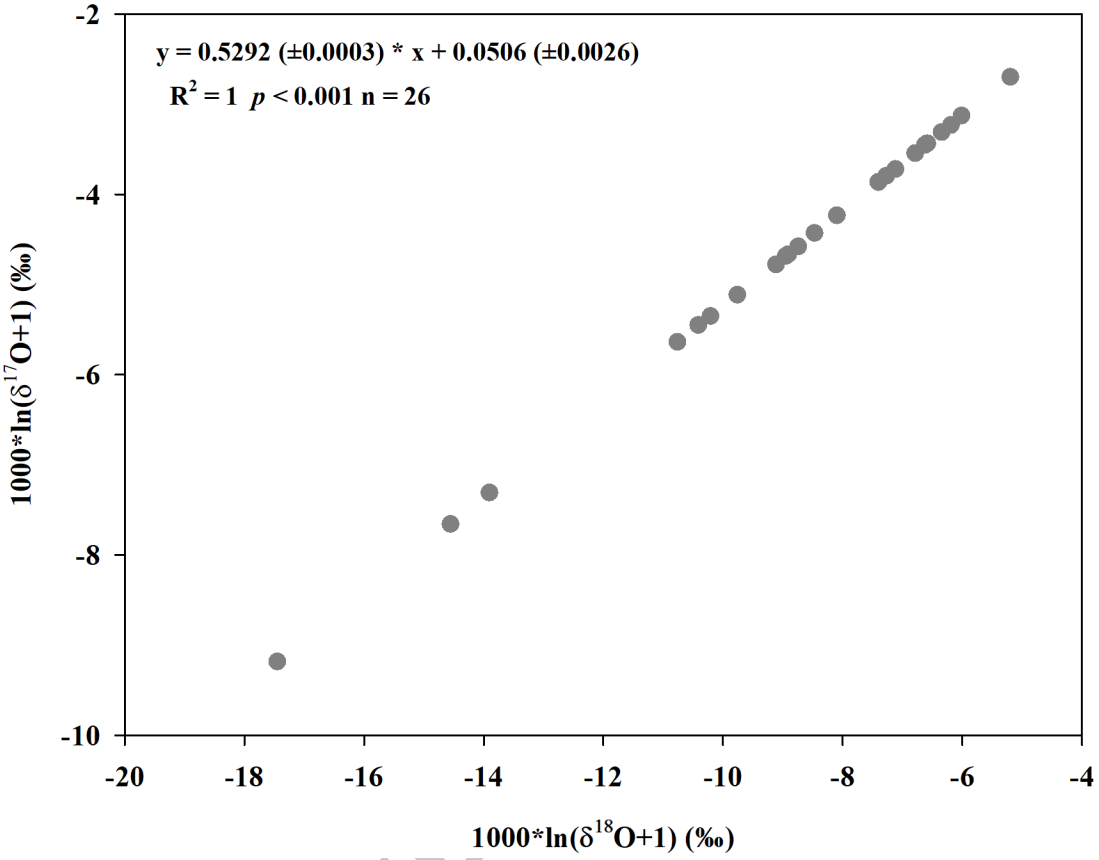

764

765 **Fig. 7 The relationships between $\delta'^{18}O$ and $\delta'^{17}O$ for precipitation-sourced tap water**
766 **samples.**

767

768

769

770

771

772

773

774

775

APPENDIX A. SUPPLEMENTARY DATA

Table A1 Summary of the precisions of δ^2H, $\delta^{18}O$, $\delta^{17}O$, and ^{17}O-excess for two international standards (SLAP and GISP) and five commercially available working standards from LGR (The number of replicates was three).

Samples	Precision			
	δ^2H (‰)	$\delta^{18}O$ (‰)	$\delta^{17}O$ (‰)	^{17}O-excess (per meg)
$SLAP_{VSMOW-SLAP}$	0.79	0.04	0.02	3
$GISP_{VSMOW-SLAP}$	0.12	0.02	0.02	7
$LGR\ \#1_{VSMOW-SLAP}$	0.80	0.06	0.03	8
$LGR\ \#2_{VSMOW-SLAP}$	0.73	0.06	0.03	2
$LGR\ \#3_{VSMOW-SLAP}$	0.42	0.01	0.02	12
$LGR\ \#4_{VSMOW-SLAP}$	0.07	0.06	0.02	8
$LGR\ \#5_{VSMOW-SLAP}$	0.72	0.06	0.03	5

Note: Standard Light Antarctic Precipitation (SLAP); Greenland Ice Sheet Precipitation (GISP); Vienna Standard Mean Ocean Water (VSMOW); Los Gatos Research Inc. (LGR).

800 **Table A2 Aridity index of tap waters from surface water-dominated sites (23 sites).**

801

City	Region	Longitude (°)	Latitude (°)	Aridity Index
Heihe	NE	127.49	50.24	0.56
Changchun	NE	125.32	43.89	0.53
Longnan	N	104.93	33.39	0.43
Pingliang	N	106.68	35.54	0.45
Hanzhong	N	107.03	33.08	0.79
Delingha	QP	97.36	37.37	0.12
Gannan	QP	102.51	35.20	0.51
Nyingchi	QP	94.48	29.58	0.51
Baotou	NW	109.85	40.67	0.19
Enshi	SE	109.48	30.27	1.29
Nantong	SE	120.86	32.02	0.88
Quzhou	SE	118.87	28.96	1.23
Lishui	SE	119.92	28.45	1.14
Fuzhou	SE	119.30	26.08	1.02
Longyan	SE	117.03	25.11	1.10
Shaoguan	SE	113.61	24.81	1.15
Nanning	SE	108.31	22.81	1.03
Tongren	SW	109.19	27.72	1.09
Bose	SW	106.61	23.90	1.01
Baoshan	SW	99.17	25.12	0.74
Simao	SW	100.98	22.80	1.05
Wenshan	SW	104.24	23.37	1.10
Bijie	SW	105.28	27.31	1.01

802

803

804

805 **Table A3 The relationships between the annual tap water isotopes ($\delta^{18}O$), d-excess and local**
806 **geographical and meteorological data at the national scale. "--" indicates the insignificant**
807 **correlation.**

		Longitude	Latitude	Altitude	Temperature	Precipitation	Relative Humidity
$\delta^{18}O$	R^2	0.16	0.16	0.31	0.28	0.31	0.32
	p	<0.001	<0.001	<0.001	<0.001	<0.001	<0.001
d-excess	R^2	0.18	0.08	0.06	--	0.05	--
	p	<0.001	0.005	0.014	--	0.031	--

808

809

Table A4 The relationships between $\delta^{18}O$, d-excess, and ^{17}O-excess and both local geographical and meteorological data at the national scale and in different regions based on linear stepwise regression analysis for both tap water and annual precipitation-sourced samples. "--" indicates the insignificant correlation.

Sample	Spatial scale	Temporal scale		^{17}O-excess	$\delta^{18}O$	d-excess
Tap water	All regions (92 sites)	Annual	model	^{17}O-excess=0.002MAP+37.38	$\delta^{18}O$ =-0.14LAT-0.002ALT -3.16	d-excess=0.10MARH-0.28MAT+0.003MAP -0.26LON+31.99
			R^2	0.08	0.46	0.39
			p	0.006	<0.001	<0.001
	QP region (6 sites)	Annual	model	^{17}O-excess=1.25LAT-4.94	$\delta^{18}O$ =-0.007ALT+8.52	d-excess =-0.005ALT +28.97
			R^2	0.89	0.84	0.82
			p	0.005	0.01	0.013
	NW region (5 sites)	Summer	model	^{17}O-excess=-2.15T_{summer}+96.24	$\delta^{18}O$ =-0.28P_{summer}-2.30	--
			R^2	0.79	0.79	--
			p	0.043	0.042	--
Precipitation-sourced sample	All precipitation-sourced regions (26 sites)	Annual	model	^{17}O-excess=-0.002ALT+41.88	$\delta^{18}O$ = 0.002MAP + 0.71MARH – 23.26	--
			R^2	0.21	0.77	--
			p	0.02	<0.001	--
	All precipitation-sourced regions except QP region (23 sites)	Annual	model	--	$\delta^{18}O$ = 0.001MAP+0.19MAT - 13.04	d-excess = 0.002MAP + 8.21
			R^2	--	0.70	0.17
			p	--	<0.001	0.048
	Precipitation-sourced sample in SE region (13 sites)	Annual	model	--	--	d-excess=-0.37MARH +40.40
			R^2	--	--	0.34
			p	--	--	0.035
	Precipitation-sourced sample in SW region (6 sites)	Annual	model	--	--	d-excess=-0.002ALT +1.07LAT-14.53
			R^2	--	--	0.995
			p	--	--	0.000

816 **Table A5 The relationships between mean annual $\delta^{18}O$, d-excess, and ^{17}O-excess and both local geographical and meteorological data at**
817 **the national scale and in different regions based on simple linear regression analysis for precipitation-sourced samples. "--" indicates the**
818 **insignificant correlation.**

819

Region	Variation		Longitude	Latitude	Altitude	Temperature	Precipitation	Relative Humidity
All precipitation-sourced regions (26 sites)	$\delta^{18}O$	R^2	0.17	0.27	0.53	0.52	0.53	0.69
		p	0.04	0.007	<0.001	<0.001	<0.001	<0.001
	^{17}O-excess	R^2	--	--	0.21	--	--	--
		p	--	--	0.02	--	--	--
All precipitation-sourced regions except QP region (23 sites)	$\delta^{18}O$	R^2	--	0.52	--	0.61	0.52	0.41
		p	--	<0.001	--	<0.001	<0.001	0.001
	d-excess	R^2	--	--	--	--	0.17	--
		p	--	--	--	--	0.048	--
Precipitation-sourced sample in SE region (13 sites)	d-excess	R^2	--	--	--	--	--	0.34
		p	--	--	--	--	--	0.035
Precipitation-sourced sample in SW region (6 sites)	d-excess	R^2	--	0.77	--	--	--	--
		p	--	0.021	--	--	--	--

820

821 **Table A6 The range and arithmetic mean values of ^{17}O-excess variations, geographical, meteorological variables, and moisture sources for**
822 **tap waters in six different geographical zones and different seasons. N, NE, NW, QP, SE, and SW was northern, northeastern,**
823 **northwestern, Qinghai-Tibet Plateau, southeastern, and southwestern, respectively. Numbers in the parentheses are mean seasonal and**
824 **annual values at different seasons and annual scale, respectively.**
825

Region	Season	^{17}O-excess (per meg)	Longitude (°)	Latitude (°)	Altitude (m)	Temperature (°C)	Precipitation (mm)	Relative Humidity (%)	Moisture sources
N	Winter	30~58 (40±8)	104.18~121.38	33.08~42.27	5~1905 (447)	-7.0~5.0 (0.5)	1~50 (14)	38.5~72.5 (51.4)	NA
	Spring	28~49 (38±5)	103.75~121.38	33.08~42.27	5~1905 (521)	8.8~16.9 (13.7)	38~265 (122)	32.9~71.2 (53.6)	NA
	Summer	22~49 (39±6)	104.18~121.38	33.08~42.27	5~1905 (485)	18.8~27.1 (24.3)	104~506 (267)	54.1~76.9 (66.5)	NA
	Fall	34~50 (39±5)	103.75~121.38	33.08~42.27	5~1905 (581)	7.1~16.5 (13.1)	50~282 (148)	57.5~84.8 (71.3)	NA
	Annual	33~48 (39±4)	103.75~121.38	33.08~42.27	5~1905 (503)	7.4~15.9 (12.7)	189~925 (539)	47.1~75.6 (60.2)	West Pacific (Liu et al., 2014)
NE	Winter	30~48 (37±7)	121.60~126.64	38.92~45.74	18~227 (107)	-14.6~-0.7 (-8.3)	16~60 (39)	53.4~67.1 (61.0)	NA
	Spring	19~41 (31±8)	121.60~127.49	38.92~50.24	18~273 (118)	3.3~11.5 (8.8)	58~173 (102)	32.9~61 (48.3)	NA
	Summer	26~43 (33±8)	121.60~127.49	38.92~50.24	21~273 (135)	20.7~23.8 (22.8)	241~457 (321)	63.1~74.8 (70.2)	NA
	Fall	27~43 (35±7)	121.60~127.49	38.92~50.24	21~273 (135)	2.3~13.3 (7.6)	31~131 (77)	48.7~66.4 (60.4)	NA
	Annual	26~48 (35±7)	121.60~127.49	38.92~50.24	18~273 (132)	2.0~12.0 (7.5)	414~909 (573)	47.6~67.9 (60.1)	North Pacific (Chen et al., 2010)
NW	Winter	26~43 (35±7)	75.99~116.07	38.47~45.60	410~1296 (977)	-13.7~-7.2)	1~41 (12)	41.7~70.7 (56.1)	High-latitudinal Arctic Ocean and Westerly water vapor (Liu et al., 2009; Liu et al., 2008a)
	Spring	37~49 (42±4)	75.99~116.07	38.47~45.60	410~1470 (1050)	5.6~16.7 (12.1)	7~80 (30)	26.9~39.9 (34.2)	Westerly water vapor, Indian Ocean, Bay of Bengal and Arabian Sea (Liu et al., 2008a)
	Summer	34~51 (42±6)	75.99~98.51	39.47~45.60	410~1470 (1045)	21.3~27.9 (25.4)	25~42 (31)	28.5~44.5 (37)	Westerly water vapor, Bay of Bengal and West Pacific Ocean (Liu et al., 2009; Liu et al., 2008a)
	Fall	32~41 (37±5)	75.99~86.13	39.47~45.60	410~1296 (938)	9.5~12.8 (11.5)	3~48 (28)	46.8~56.5 (51.7)	High-latitidinal Siberian and Mongoloa water vapor (Liu et al., 2009; Liu et al., 2008a)

									Westerly water vapor, High-latitudinal Arctic Ocean
		32~47			410~1470	3.5~13.2	60~586	41.6~59.7	and Local recycled vapor
	Annual	(40±5)	75.99~116.07	38.47~45.60	(1034)	(8.9)	(214)	(49.0)	(Li et al., 2012; Liu et al., 2014)
		25~43			2261~3657	-7.0~2.4	2~24	25.1~51.1	
QP	Winter	(35±7)	91.13~102.51	29.58~37.37	(3006)	(-3.7)	(10)	(38.6)	NA
		31~43			2261~3657	4.5~10	9~174	23.2~61.8	
	Spring	(36±4)	91.13~102.51	29.58~37.37	(3006)	(7.9)	(68)	(41.8)	NA
		28~48			2261~3657	12.1~17.8	51~563	34.6~73.4	
	Summer	(41±7)	91.13~102.51	29.58~37.37	(3006)	(15.7)	(234)	(54.9)	NA
		30~42			2261~3657	4.9~10.3	9~189	34.9~70.3	
	Fall	(38±5)	91.13~102.51	29.58~37.37	(3006)	(7.4)	(75)	(51.6)	NA
									Southern part of the plateau: Indian Ocean,
									Bay of Bengal and the Arabian Sea; Northern part of
		31~43			2261~3657	3.6~9.5	73~934	30.4~62.9	the plateau: Local recycled vapor
	Annual	(38±5)	91.13~102.51	29.58~37.37	(3006)	(6.8)	(388)	(46.7)	(Liu et al., 2014; Liu et al., 2008b)
		35~54			5~421	3.7~16.5	38~227	64.4~81.4	
SE	Winter	(45±6)	108.31~121.47	21.19~33.39	(74)	(9.8)	(135)	(70.8)	NA
		29~55			5~421	14.1~26.1	99~1076	70.3~87	
	Spring	(42±6)	108.31~121.47	20.03~33.39	(74)	(18.9)	(456)	(78.1)	NA
		34~46			5~365	25.4~29.2	354~1149	74.4~85.3	
	Summer	(41±4)	108.31~121.47	20.03~33.39	(73)	(27.5)	(694)	(79.8)	NA
		35~49			5~365	17.4~26.5	207~773	69.3~86.8	
	Fall	(42±5)	108.31~121.47	20.03~33.39	(75)	(21.9)	(413)	(79.8)	NA
		34~55			5~421	15.1~25.1	1136~2895	71.2~83.2	South China Sea and West Pacific
	Annual	(42±5)	108.31~121.47	20.03~33.39	(74)	(19.1)	(1667)	(77.3)	(Liu et al., 2014; Xie et al., 2011)
		25~51			157~1907	5.2~14.4	8~156	52.3~83.0	Westerly water vapor and Local recycled vapor
SW	Winter	(38±8)	99.17~109.19	22.8~30.66	(1171)	(9.6)	(69)	(69.9)	(Zhang et al., 2010)
		31~45			141~1907	14.7~24.9	57~403	35.1~81.1	
	Spring	(37±5)	99.17~109.19	22.8~30.66	(1099)	(19.3)	(193)	(64)	NA
		28~46			141~1907	20.5~27.8	448~712	65.4~84.9	South China Sea, Bay of Bengal and the Arabian Sea
	Summer	(37±5)	100.98~109.19	22.8~30.66	(978)	(23.6)	(603)	(78.2)	(Zhang et al., 2010)
		36~44			141~1907	15.4~23.2	192~447	66.5~86.3	
	Fall	(40±3)	99.17~109.19	22.80~30.66	(1033)	(18.2)	(300)	(80.8)	NA
		30~43			141~1907	13.9~22.6	832~1482	56.6~83.1	Indian ocean, Bay of Bengal, the Arabian Sea and
	Annual	(38±4)	99.17~109.19	22.80~30.66	(1100)	(17.7)	(1154)	(73.0)	South China Sea (Chen et al., 2010; Zhang et al., 2010)
						-			
		25~58			5~3657	13.7~17.3	1~357	25.2~84.1	
All	Winter	(40±8)	75.99~126.64	21.19~45.74	(690)	(2.9)	(83)	(64.3)	High-latitudinal Siberia (Liu et al., 2014)
		19~55			5~3657	3.3~26.1	7~1076	23.2~87	
	Spring	(38±6)	75.99~127.49	20.03~50.24	(673)	(15.1)	(214)	(59)	NA

Summer	**22~51 (38±6)**	**75.99~127.49**	**20.03~50.24**	**5~3657 (701)**	**12.1~29.2 (24.2)**	**25~1149 (417)**	**28.5~85.3 (68.9)**	**Indian Ocean and the Pacific Oceans (Liu et al., 2014)**
Fall	**27~50 (39±5)**	**75.99~127.49**	**20.03~50.24**	**5~3657 (742)**	**2.3~26.5 (15.1)**	**3~773 (220)**	**34.9~86.8 (71)**	**NA**
Annual	**26~55 (39±5)**	**75.99~127.49**	**20.03~50.24**	**5~3657 (660)**	**2.0~25.1 (13.9)**	**60~2895 (899)**	**30.4~83.2 (64.6)**	**South China Sea, Indian and the Pacific Oceans (Araguás-Araguás et al., 1998; Liu et al., 2014)**

826

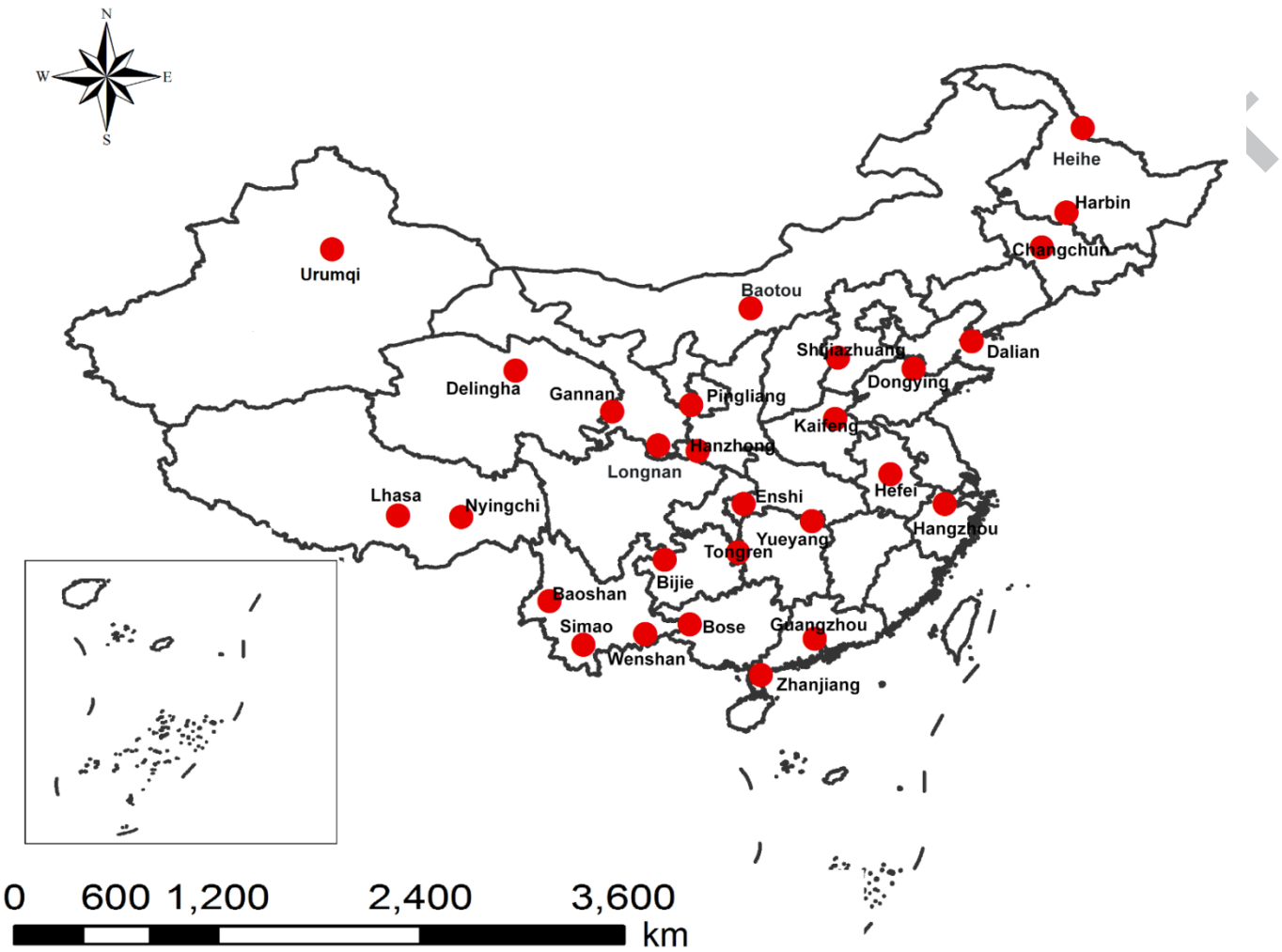

827

828 **Fig. A1 The locations of tap water and precipitation-sourced samples with names mentioned in the main text.**